Journal of Analytical and Applied Pyrolysis 181 (2024) 106591

Contents lists available at ScienceDirect

Journal of Analytical and Applied Pyrolysis

journal homepage: www.elsevier.com/locate/jaap

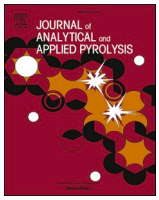

Identification of a polyfuran network as the initial carbonization intermediate in cellulose pyrolysis: A comparative analysis with cellulosic hydrochars

Lukas Fliri [a,*], Kseniia Dubivka [a], Dmitrii Rusakov [a], Alexander Volikov [b], Chamseddine Guizani [c], Sami Hietala [d], Svitlana Filonenko [b], Michael Hummel [a,*]

[a] Department of Bioproducts and Biosystems, Aalto University, P.O. Box 16300, Aalto 0076, Finland
[b] Max-Planck Institute of Colloids and Interfaces, Am Mühlenberg 1, Potsdam 14476, Germany
[c] VTT Technical Research Centre of Finland, Tietotie 2, Espoo FI-02150, Finland
[d] Department of Chemistry, University of Helsinki, P.O. Box 55, Helsinki 00014, Finland

ARTICLE INFO

Keywords:
Cellulose dehydration
Polyfurans, humin
Char

ABSTRACT

Pyrolysis of cellulose is accompanied with different complex and superimposing transformations resulting in a broad mixture of isolable products with strong variations depending on the applied reaction conditions. The operative chemistry represents a challenge for analytical chemists and process engineers alike. Especially, the reactions leading to char formation cannot be described as sufficiently understood. In ongoing efforts to shed light on the major transformations during charring of cellulose, the occurrence of a thermostable condensed phase (TSCP) previously postulated as an important carbonization intermediate formed below 300 °C was revisited. It was attempted to isolate pure TSCP intermediates without cellulose contamination by applying dehydration catalysts known from cellulose based carbon fiber production and extensive isothermal treatments. It was shown that the weight loss levels off during isothermal treatment for 6 h in the temperature range of 200–250 °C, resulting in the formation of a common intermediate with an almost identical composition – irrespective of the employed temperature or catalyst. Moreover, isothermal treatment of pure cellulose at 270–280 °C for up to 12 hours also resulted in the formation of an intermediate which had a similar composition as the material prepared with added dehydration catalysts. To test the hypothesis of a proposed polyfuranic nature of the TSCP intermediate the prepared samples were compared with hydrochars obtained from hydrothermal treatment of cellulose as reference material for a polyfuranic humin. Similarities and differences are discussed and implications for the overall carbonization mechanism are summarized.

1. Introduction

The pyrolysis of wood biomass was among the first chemical processes conducted in human history. Thereby produced charcoal or tar were used extensively in preindustrial times either as fuel or in materials applications [1,2]. More recently the pyrolysis of biomass received renewed attention within diverse research communities working with biofuels or bio-based carbon materials [3–13]. Given the complex product mixtures resulting from the pyrolysis of wood, several attempts have been made to fractionate lignocellulosic biomass into its major constituents and study their pyrolytic transformations separately. Thereby, cellulose as the major constituent of wood received special attention. Its pyrolysis behavior was investigated in numerous fundamental studies and the operative kinetics and thermodynamics can be accurately described by two-pathway pyrolysis models [14–24]. Nonetheless, the complex chemistry behind the heat treatment of cellulose, especially the reactions leading to char formation are far from being sufficiently understood. This was for example acknowledged by Dauenhauer *et al.* as one of the top ten fundamental unsolved challenges in biomass pyrolysis back in 2012 [7]. With regards to our group's ambition to use regenerated cellulose fibers as cost competitive precursors to bio-based carbon fibers (CFs), this knowledge gap represents a particular and important research problem [25–28]. Without pretreatment, CF yields are usually low (5 – 10 wt%), even upon slow pyrolysis

* Corresponding authors.
E-mail addresses: lukas.fliri@aalto.fi (L. Fliri), michael.hummel@aalto.fi (M. Hummel).

https://doi.org/10.1016/j.jaap.2024.106591
Received 5 April 2024; Received in revised form 7 June 2024; Accepted 10 June 2024
Available online 11 June 2024

[29–32]. Furthermore, the resulting oxygen containing carbon networks exhibit mechanical properties which do not meet the required standards for application in the automotive or civil engineering industries [30, 33–35]. Process adaptations will be required to increase the CF yield and decrease the defects in the resulting carbon structures.

The fact that the char forming reactions during cellulose heat treatment are still debated is largely related to its intrinsic pyrolysis behavior and the associated analytical limitations. When treating pure cellulose in a classical thermogravimetric analysis (TGA) experiment under inert conditions and at a constant heating rate, its weight loss is marginal up-to around 250 °C before a rapid thermal degradation occurs between 250 and 400 °C. Beyond this temperature, the weight loss in the charred residue becomes marginal again [36]. This reverse sigmoid curve translates into one sharp peak in the differential DTG plot occurring around 300–350 °C – with variations depending on the heating rate and cellulose source – in which both the major tar forming reactions and the initial char formation with associated secondary reactions superimpose (Fig. 1A). This leads to significant overlap of analytes stemming from the different pathways when thermal analysis is coupled with evolved gas analysis (EGA) techniques. Consequently, thermal analysis as one of the main tools in pyrolysis research only gave limited information on the minor char forming pathway during cellulose pyrolysis.

Residual solid fractions were isolated and investigated independently by various techniques to get a better understanding of their composition [37–44]. Given the reluctant solubilization behavior of both cellulose and the resulting charred material, these studies significantly relied on semi-quantitative spectroscopic techniques such as IR or solid state ^{13}C NMR [37–43], or destructive procedures like curie point pyrolysis GC/ MS [39,44]. The focus was set on the initial char forming reactions occurring below a temperature of approximately 400 °C. Even when conditions favoring the char forming reactions are chosen for sample preparation (*i.e.*, low heating rates or isothermal steps), the exact experimental conditions can still vary significantly. These differences in sample preparation led to conflicting reports in literature. For example, solid state ^{13}C NMR spectra reported by Liang *et al.* suggested that cellulose remains almost intact after "slow pyrolysis" up to a temperature of 325 °C [45]. In contrast Pastorova *et al.* reported significant changes in their spectra after isothermal treatment for 2.5 h at a temperature of 270 °C [39]. The heat treatment at temperatures where first changes can be observed is often insufficient, which results in thermostabilized materials strongly resembling the cellulosic starting material. Contrary, signals for aryl structures can be observed when the applied temperature exceeds approximately 300–350 °C (Fig. 2) [39,46]. During preparation of cellulose based carbon fibers, the occurring transformations are commonly treated as a multistep process. The reactions leading to initial dehydrated char precursors below around 300 °C are proposed as the major yield determining step, followed by aromatization occurring between 300 – 600 °C and formation of the polycondensed turbostratic carbon network and graphitization at higher temperatures [33,34,41, 42]. To the best of our knowledge, there is no study investigating the presumed first two subsequent reaction steps independently. The initial char forming reactions below 300 °C are also of central interest for CF production to increase the final char yield. Different thermostabilization pretreatments include slow heating rates, isothermal treatments, or addition of dehydration catalysts and are usually all applied at temperatures below 300 °C before the volatilization caused by unzipping reactions becomes significant [29–32]. For example, isothermal treatment of cellulose for 16 h at 230 °C almost doubled the ultimate char yield at 1200 °C [47]. This means that the onset temperature of the initial charring reactions must lie well below the often-reported degradation peak around 300 °C. However, these transformations occur at an exceptionally slow rate. This aspect of cellulose pyrolysis complicated the clear separation and investigation of the formed intermediate structures so far. This issue was highlighted in early literature. For isothermal treatment of pure cellulose at 250 °C under inert conditions a constant weight was only observed after around 180 h [21]. During isothermal treatment in vacuum at 226 °C the weight did not stabilize even after 1000 h [48].

The transformation from a carbohydrate to a carbon material must inevitably include the release of water. Dehydration is often associated with the initial reactions in the char forming pathway [49]. However, given all the mentioned analytical limitations and simultaneously occurring reactions, complete mechanistic schemes for cellulose dehydration are scarce. To the best of our knowledge only one complete reaction scheme for the transformation of cellulose to a carbon network was postulated by Tang and Bacon in the 1960's [41]. Based on IR studies, a dehydration directly from the glycopyranose units *via* elimination reactions was proposed [41]. The formed carbonyl and alkene bearing anhydro saccharide structures were postulated to undergo a transition to a "4 carbon" intermediate which serves as the key building block of the aromatic network. While this stepwise dehydration – aromatization – carbonization regime is still widely accepted, the postulated structures could not be validated thus far. Notably, this mechanism is still widely cited in the cellulose carbonization community [33,34], while it is disregarded in respected reviews from leading researchers focusing on volatile pyrolysis products [7,50,51]. Different causes for char formation were suggested, mostly favoring crosslinking or polycondensation reactions [7,50,51]. However, none of these alternative proposals was composed to a complete mechanistic scheme and probable intermediate structures are seldomly discussed in more detail.

Our group recently re-investigated the chemical reactions caused by isothermal treatments of cellulose fibers up to 250 °C for several hours by solution state NMR spectroscopy [52]. Thereby, no dehydration within the glycopyranose repeating units was evident [52]. Instead, only partial depolymerization through intramolecular chain scission to

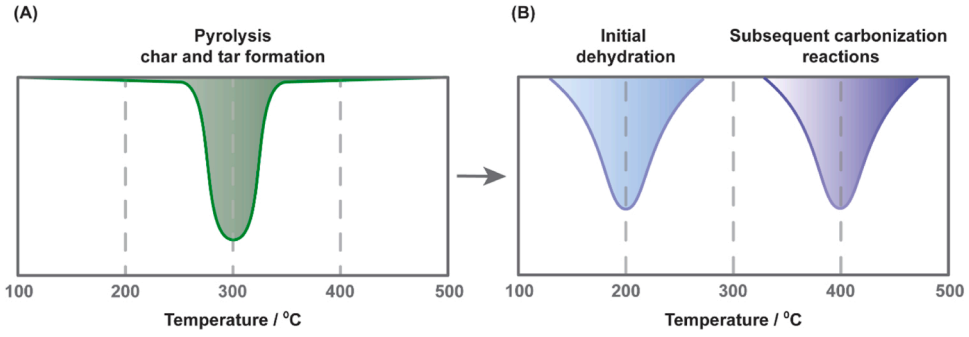

Fig. 1. Simplified schematic of DTG thermograms obtained in this study. A) The pyrolysis of pure cellulose is associated with one sharp DTG maximum occurring around 300 °C, in which both the char and tar forming pathways are summarized (Fig. S1). B) Through application of long isothermal treatments and / or dehydration catalysts it was possible to isolate the initial dehydration reactions (Fig. S1). This allowed to investigate the subsequent carbonization reactions independently (Figs. S33 and 34).

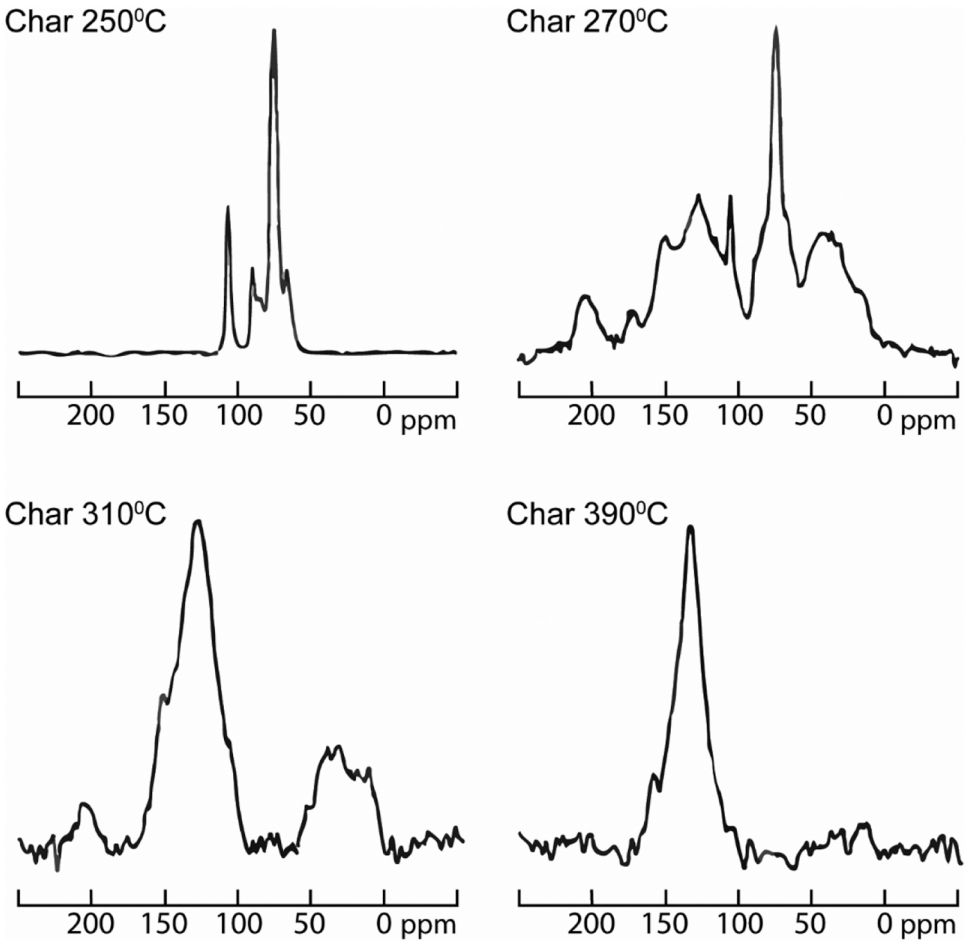

Fig. 2. Solid state ^{13}C NMR spectra for Avicel MCC thermostabilized under N_2 for 150 min at the respective temperatures as reported by Pastorova et al. [39] While at 250 °C the isolated material resembled the MCC starting material, at 270 °C clear changes due to the formation of a thermostable condensed phase became apparent, although superimposed with cellulose resonances. At 310 °C subtle peaks in the carbonyl and alkyl area reminiscent of TSCP are still visible, while aryl peaks like the ones observed in the char at 390 °C start to dominate the spectrum. Reprinted from Pastorova *et al.* (1994) with permission from Elsevier.

oligomeric cellulose structures with terminal levoglucosan (LGA) units at the reducing end groups (REGs) was observed. Size exclusion chromatography (SEC) also hinted towards crosslinking of the oligosaccharide structures [52]. These moieties are usually more connected to the tar forming pathway [41] and do not serve as a plausible direct explanation for increased char formation [51]. The localization of the observed reactions is noteworthy under the aspect that cellulose REGs were reported to have a considerable effect on the thermal stability of cellulose [53–56]. Further, there are clear similarities in the chars prepared from cellulose and LGA [57]. In a follow up-study the importance of REGs during char formation was confirmed in the significantly higher char yields of thermostabilized electron beam irradiated cellulose fibers [58].

However, in both studies conducted in our group analytical difficulties were encountered when applying solution state techniques, due to the formation of a recalcitrant insoluble phase [52,58]. In an acid hydrolysis study conducted by Pastorova *et al.* similar problems were encountered. There, the insoluble fractions were termed as thermostable condensed phase (TSCP) and postulated to be an important carbonization intermediate [39,59]. In the initial study it was suggested that TSCP must be characterized as a "new polymer" with furanoid skeletons, hydroxyaromatic skeletons, unsaturated hydrocarbon chains, carbonyl and carboxylate functionalities [39]. Furthermore, a reaction sequence from pyranose over intermediate furan structures to benzylic moieties in the carbonized material was proposed. However, their samples obtained below 300 °C contained considerable fractions of cellulosic starting material, which complicated the unambiguous characterization of a first intermediate (Fig. 2).

Noteworthy, furan moieties are considered as general pyrolysis and carbonization intermediates of different saccharides [60]. They recently received increased attention in the context of hydrothermal biomass conversion [61]. During monosaccharide valorization, polyfurans are often observed as unwanted by-products in the production of 5-hydroxymethylfurfural (5-HMF), which are commonly referred to as humins [62]. The insoluble, polymeric structures result from a complex polycondensation of 5-HMF with reactive side products [62–66]. Using similar experimental setups, the targeted production of hydrochars from lignocellulosic biomass was investigated [67–69]. The exact constitution of these polyfuranic materials depends on the starting materials and applied process parameters and often aryl moieties are also incorporated in the structures [67–69]. Overall, the composition of bioderived polyfurans seems so far not well defined and incorporates a broad spectrum of structures which are still actively investigated [62,67]. Nonetheless, suitable analytical techniques were applied to investigate different insoluble humins and sophisticated structural proposals exist for certain derivatives [70–73].

Dauenhauer *et al.* implied that a humin might also form during dry cellulose carbonization and that the occurring reactions might resemble the transformations during hydrothermal treatments [7]. While to the best of our knowledge no direct comparison between the two carbonization conditions was conducted yet, studies supporting this hypothesis were reported. For example, Kawamoto and his coworkers recently

compared the products of thermally copolymerized 5-HMF and glycerol with thermostabilized cellulose [74]. Owing to the evident similarities they proposed the formation and polycondensation of 5-HMF with aliphatic alcohols (*i.e.*, saccharides or their fragmentation products) as first step in the dry carbonization sequence of cellulose. Moreover, an autocatalytic reaction progress caused by the released water was proposed. The self-acceleration of cellulose dehydration was also observed previously [49] and connected to the catalytic action of generated fragmentation products [23]. In his seminal review, Kawamoto also pointed out that the formation of 5-HMF structures is conceivable by the dehydration of the REGs, proceeding over stabilized intermediates [51]. In turn, release of water *via* simple elimination reactions from vicinal diols as present in the glycopyranose units [41] should not be energetically accessible below 350 °C [51,75]. The selective dehydration of REGs to 5-HMF structures was also described in the older cellulose pyrolysis literature, but not directly associated with the major char forming reactions [49]. Overall, a localized dehydration causing an autocatalytic reaction progress *via* continuous liberation of REGs [74] would be in line with the observed general importance of REGs during cellulose carbonization [53–58] and with the reaction sequence pyranose to furan to benzene proposed by Pastorova *et al.* [39,59]. In addition, clear similarities in the reported FTIR and solid state ^{13}C NMR spectra are discernible when comparing celluloses thermostabilized below 300 °C [30,39] with humins derived from hydrothermally treated sugars [72,73] or isolated hydrochars prepared from cellulose [67,68].

In conclusion, circumstantial evidence for the participation of furans [76] or humin-like substances [7,30,39,74] in the carbonization mechanism of cellulose was reported. However, an entirely clear and convincing experimental validation for the connection between thermostabilized cellulose and a polyfuran is still missing. Our aim in this study was to isolate and characterize the postulated TSCP intermediate in a purer form without residual cellulose constituents and at temperatures before further reactions to benzene moieties become significant. For this endeavor, different isothermal treatments up to 12 hours in the temperature area from 200 to 280 °C were applied to a Avicel® PH-101 microcrystalline cellulose (MCC) model compound [77] until the weight loss leveled-off. To accelerate the process, dehydration catalysts commonly employed in the preparation of cellulose-based carbon fibers were added for the lower investigated temperatures [30,78]. The isolated TSCP samples were analyzed by various means. The results were compared with hydrochars prepared from the same cellulose source and with data of differently prepared humins reported in literature [68,72,73].

2. Materials and methods

All employed chemicals were sourced from commercial sources (Merck Sigma Aldrich) and used without further purification. Deionized water was used to dissolve or dilute the used dehydration catalysts (H_2SO_4, $(NH_4)_2HPO_4$, ammonium *p*-toluenesulfonate) [30,78] and prepare 10 % (w/w) stock solutions. Avicel® PH-101 microcrystalline cellulose (MCC) was used as a well-studied cellulosic model substance throughout the study [77].

2.1. Application of dehydration catalysts

Avicel® PH-101 was suspended in a stock solution of the respective dehydration catalyst (10 % w/w) in a solid to liquid ratio of 1 g per 10 mL. The suspension was stirred in the open at room temperature (20 °C) for 10 min and filtered off under vacuum. The isolated solids were dried at a maximum temperature of 55 °C in a standard drying oven until a constant weight was reached. The dried samples were stored in a desiccator over silica. The drying caused a discoloration of the material from white to brown / black for the H_2SO_4 treated sample. According to solution sate NMR spectra no significant transformations of the bulk material to dehydrated saccharides or insoluble carbonization intermediates occurred [52]. The change in color can be assigned to minor chromophore formation on the cellulose surface. However, minor peaks for sulfate half ester groups in the diffusion edited ^1H spectra indicated the occurrence of covalent modification during drying [79]. Obtained analytical data for the differently treated MCC starting materials is summarized in the supporting information in Tables S1 and S2 and Figures S1–14.

2.2. Preparation of TSCP samples from MCC

For the preparation of the TSCP materials either a Nabertherm RHTH 80–300/16 tube furnace or a NBD Tech USA NBD-O1200–50IC tube furnace was used. Both ovens were operated under a N_2 flow of 4–5 L/h (70–80 mL/min) with a heating rate of 5 K min^{-1} to the preset isothermal temperature step. Before the heat treatment ~400 mg of pure MCC or MCC pretreated with dehydration catalyst were weighed into a conical crucible. Two crucibles filled with the same starting material were placed in the furnace at a defined distance to the temperature sensor. The materials were heated for 6 h and 12 h using isothermal treatments between 250 and 280 °C in case of pure MCC, or for 0.5 h, 1 h, 3 h and 6 h using isothermal treatments between 200 and 280 °C in case of MCC treated with dehydration catalyst. The samples were removed from the oven following a cooling down period when the samples reached a temperature below 100 °C. The prepared samples are summarized in Table 1. The obtained yields and key analytical data are summarized in the supporting information in Tables S5–8 and Figures S19–29. All materials were stored in a desiccator over silica. The TSCP samples were labeled according to the following sample code: **TSCP_** [applied dehydration catalyst (**P** = pure MCC; **SA** = H_2SO_4; **AP** = $(NH_4)_2HPO_4$; **AT** = ammonium *p*-toluenesulfonate)] _ [temperature of isothermal step (°C)] _ [time kept at isothermal step (h)].

2.3. Preparation of hydrochars

Hydrochar samples were prepared through hydrothermal treatment of MCC in water under varying pH conditions and for different durations. Five syntheses were conducted. The reaction time and the mixture compositions are listed in Table S3. The reaction mixtures were transferred to 50 mL pressure vessels lined with removable polytetrafluoroethylene (PTFE) cups from Parr (Moline, IL, USA). Hydrothermal treatment was performed in an oven (UF30, Mermet GmbH, Schwabach, Germany) for 2/4/8 h after reaching 220 °C. At the end of the reaction time, the autoclaves were cooled with ice. The resulting slurries were

Table 1
Conditions used during the preparation of the screened TSCP samples.

Series	Dehydration catalyst	Isothermal step / °C[a]	Samples drawn / h	Complete Conversion to TSCP / h[b]
TSCP_P	–	250	6, 12	–[c]
		260	6, 12	–[c]
		270	6, 12	12
		280	6, 12	6
TSCP_SA	H_2SO_4	200	0.5, 1, 3, 6	1
		210	0.5, 1, 3, 6	0.5
		220	0.5, 1, 3, 6	0.5
		230	0.5, 1, 3, 6	0.5
		240	0.5, 1, 3, 6	0.5
		250	0.5, 1, 3, 6	0.5
		260	0.5, 1, 3, 6	0.5[d]
		270	0.5, 1, 3, 6	0.5[d]
		280	0.5, 1, 3, 6	0.5[d]
TSCP_AP	$(NH_4)_2HPO_4$	250	0.5, 1, 3, 6	0.5
TSCP_AT	NH_3 *p*-TsOH	250	0.5, 1, 3, 6	0.5

[a] heating rate of 5 K min^{-1} until isothermal temperature was reached
[b] time after which no residual cellulose was determined in the samples
[c] no complete conversion achieved after longest treatment time
[d] follow-up carbonization reactions indicated by performed analyses.

dialyzed using dialysis tubes (Servapor MWCO 3500, Serva Electrophoresis GmbH, Germany) against deionized water until the solution resistance decreased below 0.1 μS. The hydrochar samples were then lyophilized (24 h, LYOTECH GT2-E benchtop freeze dryer). The hydrochars were labeled according to the following sample code: **HC_** [applied conditions (**W** = H_2O; **SA** = H_2SO_4; **KOH** = KOH)] _ [time kept in reactor (h)]. Obtained analytical data for the different prepared hydrochars is summarized in the supporting information in Table S3 and Figures S15–17.

2.4. Thermal analysis

Two different instruments were used for the thermogravimetric analysis (TGA). Initial isothermal prescreening and a non-quantitative monitoring of the expulsed gases were conducted on a Netzsch STA 449 F3 Jupiter instrument coupled with a QMS 403 Aëolos Quadro mass spectrometer. The temperature in the connecting tube was set at 300 °C. In the isothermal prescreening without MS detection a 70 mL min^{-1} N_2 flow was used. The MCC samples (~20 mg) were heated (5 K min^{-1}) from 40 °C to the isotherm between 200 and 280 °C kept isothermally for 12 h. To discern influences on the char yield the samples were subsequently heated to 600 °C (5 K min^{-1}) and kept at this temperature for 30 min (Table S4). Simultaneous thermal analysis (STA) measurements coupled with MS detection were conducted under a 70 mL min^{-1} He flow with an electron-impact (EI) ionization energy of 70 eV. Sample mass varied from 5 to 10 mg (Hydrochar) to 20–25 mg (MCC or TSCP). Two different protocols were used. In the first the samples were heated from 40 °C to 600 °C (1 K min^{-1}) and the expulsed volatiles were detected in a continuous mode by screening *m/z* values from 5 to 300 amu. In the second the samples were heated from 40 °C to 1000 °C (10 K min^{-1}) and the volatiles were measured using the multiple ion detection (MID) mode targeting *m/z* values of 2, 15, 18, 28 and 44, corresponding to H_2, CH_3, H_2O, CO and CO_2.

For the quantitative analysis of the evolved gases a Netzsch Simultaneous Thermal Analyzer STA 449F1 coupled to a mass spectrometer was used. About 10 mg of sample was heated from room temperature up to 1500°C at 10 K min^{-1} under 70 mL min^{-1} of Ar gas. The mass loss dynamics, heat flux and evolved gases were measured simultaneously;· H_2O, CO and CO_2 gases were quantified after calibration of the mass spectrometer using $CaC_2O_4 \cdot H_2O$ following a previously described protocol [80,81].

2.5. NMR spectroscopy

Solid-state ^{13}C CPMAS NMR spectra were measured with a Bruker Avance III 500 MHz NMR spectrometer using a double resonance CPMAS probehead. The samples were packed into 4 mm outer diameter ZrO_2 rotors, sealed with KEL-F endcaps and spun at spinning frequency of 12 kHz. ^{13}C CPMAS spectra were obtained at room temperature with at least 4000 scans using a 3 s relaxation delay and 3 ms contact time for cross polarization. The spectra were externally referenced to adamantane.

Solution state NMR spectra were recorded with a Bruker Avance III 400 NMR spectrometer to exclude considerable reactions of the MCC bulk material with the dehydration catalysts during the drying step. The cellulosic materials were dissolved in a P_{4444}[OAc] – DMSO-d_6 (1:4 wt %) electrolyte system following a reported protocol [82]. The spectra were recorded with a measuring concentration of 5 wt% at 65 °C.

3. Results and discussion

3.1. Preparation and identification of a pure thermostable condensed phase

3.1.1. Prescreening of applicable conditions by thermal analysis

To determine suitable time and temperature windows for the isolation of a stable carbonization intermediate without residual cellulose, both untreated and H_2SO_4-treated MCC were investigated by isothermal TGA experiments. A plateau in the isothermal TGA plots due to the levelling-off of the weight loss should indicate complete conversion into TSCP. Only minor mass decrease owing to secondary reactions was expected. As the weight loss below 250 °C was minor in our prestudy on cellulosic fibers [52], the untreated MCC was screened in the temperature range from 250 °C to 280 °C for 12 h each in 10 °C intervals (Fig. 3A). The TGA plots indicated that no full conversion was achieved after 12 h up-to an applied temperature of 260 °C. A plateau was reached at 270 °C after ~ 6 hours or at 280 °C after ~ 3 hours respectively (Table S4). There were discernible differences in the mass yield of the intermediate and the char yield after heating to 600 °C. These were ascribed to losses due to volatile formation following the tar forming pathway of cellulose. Volatilization had a more pronounced effect when the applied isothermal treatment temperature was closer to 300 °C – the lowest estimate for the debated boiling point of LGA [51]. Noteworthy, the observed char yields at 600 °C for samples where the weight loss did not level off was higher than for the ones where a complete conversion to an intermediate was observed (Table S4). This is in accordance with literature reports [47] and can be explained by the higher losses of glycopyranose moieties due to volatilization reactions already during the isothermal treatment.

Samples treated with H_2SO_4 [30] showed a significantly faster conversion at lower temperatures. Two charges of H_2SO_4-treated MCC were prepared and the TGA prescreening was conducted with **MCC_SA-1** with a determined H_2SO_4 content of 9 wt% (Table S1). Conducted TGA experiments with a heating rate of 1 K min^{-1} showed that the addition of H_2SO_4 reduced the weight loss maximum to around 145–160 °C compared to ~ 300 °C for the untreated sample (Table S1). According to evolved gas analysis (selected analytes: H_2O, CO_2, CH_3) the loss of H_2O was the major expulsed volatile between 150 and 200 °C accompanied with minor CO_2 generation (Figure S3). However, we encountered issues with the CO signal and did not monitor formation of low molecular weight oxygenated hydrocarbons, which are both likely expulsed too.

The accelerated dehydration resulted in an almost complete conversion of cellulose already during the initial heating period (5 K min^{-1}) to the preset isothermal step. The weight loss leveled off and stayed more or less constant over a period of 12 h at 200 °C (Fig. 3B). Notably, the weight yields of the plateaus for the H_2SO_4-treated samples were higher than those observed for pure MCC (*e.g.*, 51 % after 12 h at 250 °C compared to 24 % or 21 % observed for untreated MCC at 270 °C or 280 °C for 12 h respectively). This also resulted in a higher char yield observed at 600 °C and verifies the connection of the presumed intermediate with the char forming pathway (Table S4). The higher yield is ascribable to mitigated losses due to volatilization in the H_2SO_4-treated samples. The major thermal conversion occurs at temperatures below 200 °C where the evaporation of the major tar forming constituents (*e.g.*, LGA) is expected to be marginal. To discern possible influences of H_2SO_4 on the further thermal degradation of the materials, isothermal treatments were conducted at the same temperatures needed for the transformation of pure MCC (Fig. 3B). A slight reduction of the weight was observed when the applied temperature was higher than 260 °C. Although the differences were rather small, a minor influence of the dehydration catalyst on the subsequent carbonization step or secondary volatilization reactions was suggested.

3.1.2. Preparation of TSCP samples and screening of composition

The results of the TGA prescreening were adapted to prepare samples on a larger scale for subsequent chemical analysis using tube furnaces. To screen the chemical composition and determine differences between the TSCP materials, all prepared samples were colloquially investigated and compared using FTIR spectroscopy and elemental analysis. The samples obtained at the longest isothermal treatment time at the respective temperature were additionally screened by thermal analysis (Figure S33 and S34). The applied conditions are summarized in Table 1.

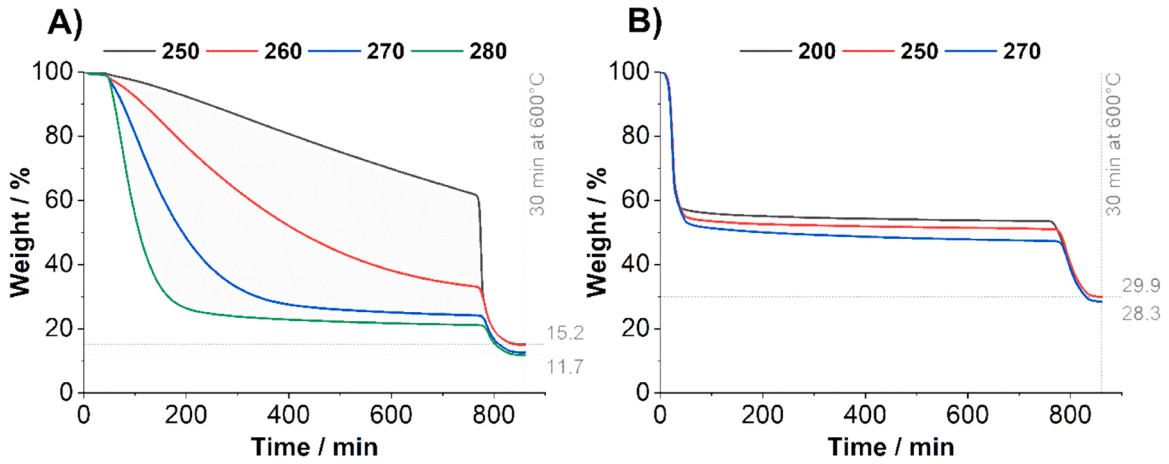

Fig. 3. TGA plots for long time isothermal treatments at the respective temperatures for A) pure MCC and B) MCC treated with H_2SO_4 as dehydration catalyst. A heating rate of 5 K min^{-1} was used for all temperature increase steps; 30 min isothermal at 600 °C added to obtain char yield; N_2 flow 70 mL/min.

Noteworthy, accurate and repeatable sample preparation on a larger scale was difficult, when using untreated MCC as substrate and the transformation to a stable intermediate was not complete (below 260 °C). There were significant variations in the obtained weight yields caused by heat- and mass transfer limitations in the oven. Repeatable results could only be achieved when the crucibles were placed at a defined distance to the temperature sensor of the oven. We compensated for this bias by positioning two crucibles side-by-side in the oven and compared the yields of them. Only when the transformation reached completion, the observed mass differences became negligible (usually around or below 1.5 wt%) and defined samples could be obtained (see Table S5). Moreover, it is noteworthy that the weight yields observed in the TGA plots and the isolated masses showed slight variations. This can be ascribed to differences in heat and mass transport phenomena influencing the extent of secondary char forming reactions in the bulk synthesis (~ 400 mg starting material) compared to the lower sample amounts used in the TGA experiments (~ 20 mg). Intriguingly, the bulk preparation of H_2SO_4 derived TSCP resulted in lower yields than in the TGA experiments, while the opposite was observed in the thermal treatment of pure MCC. The obtained weights and determined elemental compositions for all samples are summarized in the supplemental information, Tables S5–8 and Figures S19 and S22–24. The associated FTIR spectra are shown in Figures S21 and S26–29. Selected samples are presented and discussed in the main manuscript in Figs. 4 and 5.

For the samples prepared from pure MCC without addition of catalyst, materials with incomplete thermostabilization were incorporated in the experimental matrix. In the materials where no stable weight was reached the FTIR data hinted towards the presence of unreacted polysaccharidic fractions, with vibrations resembling cellulose (Fig. 4A). The presence of residual starting material was also corroborated by elemental analysis results, when plotting the elemental O/C *versus* H/C ratios in a van Krevelen diagram (Figure S20). The plot showed a linear decrease from the MCC starting material towards the completely thermostabilized intermediate suggesting dehydration as the major occurring reaction. Additionally, the presence of residual cellulosic fractions was suggested in the conducted thermal analysis in a DTG peak or shoulder around 320 °C (heating rate 10 K min^{-1}) characteristic for the pyrolysis of non-thermostabilized cellulose. Once complete conversion was achieved following treatment at either 270 or 280 °C for at least 6 h the respective changes in the FTIR spectra became minimal and the major thermal event in the DTG thermograms shifted to a broader peak with a maximum around 380–390 °C (Table 2). However, there were still small shifts in the elemental analyses results with increasing carbon and decreasing oxygen values (Table S5). It should be noted that with the employed experimental matrix it was only possible to obtain three samples of TSCP (**TSCP_P_270_12h**, **TSCP_P_280_6h** and **TSCP_P_280_12h**) where cellulose contamination could be excluded by all employed screening analytics in the case of pure MCC as starting material (Fig. 4B). Complete conversion at lower temperatures without a catalyst was not anticipated due to the necessary long preparation times

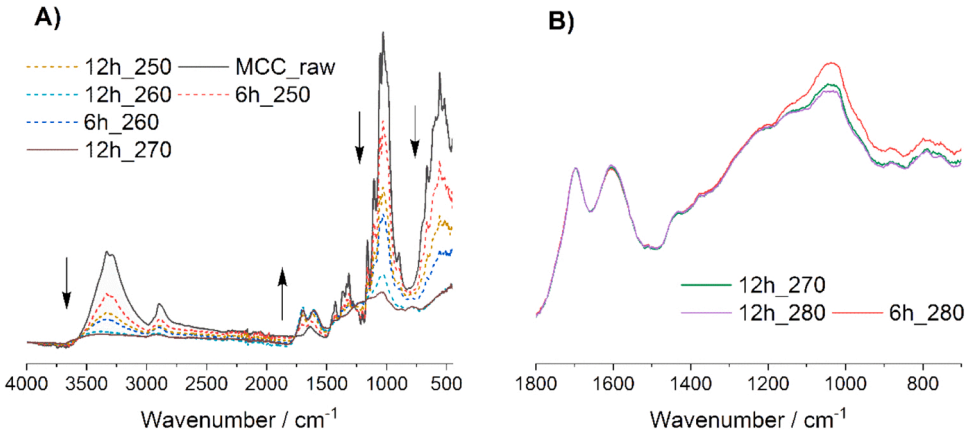

Fig. 4. FTIR spectra obtained for TSCP materials from pure MCC. A) With increasing intensity of the heat treatment (time, temperature) the characteristic cellulose vibrations diminish and the gradual formation of TSCP is indicated by the occurrence of two peaks around 1600 cm^{-1} and 1700 cm^{-1}. B) Once all cellulose constituents of the materials are transformed prolonged heat treatment did not induce further changes in the spectra.

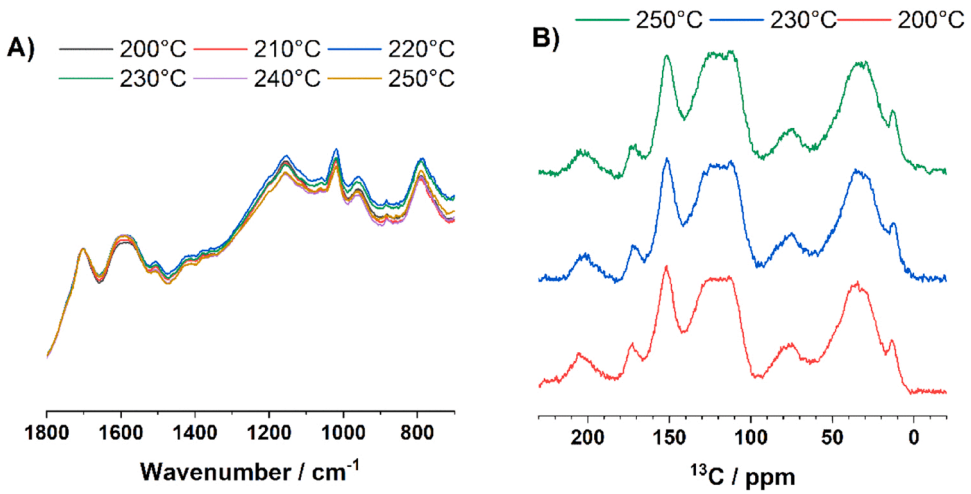

Fig. 5. A) FTIR and B) solid state ^{13}C NMR spectra obtained for representative TSCP materials prepared from H_2SO_4-treated MCC after isothermal treatments for 6 h between 200 and 250 °C. Both analytics showed that a common thermally stable intermediate with only minimal changes in the chemical composition is formed in this temperature window. Peak assignments will be discussed in the following section.

[21,48], and conversion at higher temperatures was omitted due to expected follow up reactions of the intermediate TSCP materials [39].

As expected from the TGA prescreening milder thermostabilization conditions were sufficient when adding H_2SO_4 as dehydration catalyst. All discussed samples up-to a temperature of 250 °C and samples treated for 6 h at 260, 270 and 280 °C were prepared with **MCC_SA-1**. For the materials prepared at 260–280 °C at up to 3 h, **MCC_SA-2** with a higher H_2SO_4 content of 15 wt% was used as starting material. In the FTIR spectra we could not discern obvious differences between any of the isolated H_2SO_4-treated TSCP materials, indicating the formation of a common and stable intermediate over the whole investigated temperature window (Fig. 5A and S26–29). There were no signs for residual cellulosic material in any of the FTIR spectra. There were also no discernible differences in the solid state ^{13}C NMR spectra measured for three samples treated for 6 h at 200, 230 and 250 °C, respectively (Fig. 5B). Only the thermal analyses of the samples treated at 200 °C showed a minimal bump in the DTG peaks reminiscent of residual cellulose, in connection with slightly lower char yields at 1000 °C (Figure S31). The elemental compositions for the isolated intermediates between 200 and 250 °C were in the range of 65 – 68 wt% carbon, 3.9 – 4.2 wt% hydrogen and 28 – 31 wt% oxygen (Table S6). After prolonged treatment at temperatures above 250 °C a shift of the carbon values towards 69 – 72 wt% with a decrease of the oxygen values to 24 – 27 wt % was observed while the hydrogen values did not change considerably (Table S7). This can be ascribed to both the harsher conditions and the higher catalyst loading in the used starting material. In accordance with the TGA plots this hinted towards the presence of a further slow conversion of the TSCP intermediate, presumably due to dehydration and decarboxylation reactions, which should be favored in the presence of an acid catalyst. Further conversion was also suggested when plotting the molecular O/C *versus* H/C ratios in a van Krevelen diagram (Figure S25). However, there were no striking differences between the FTIR spectra of TSCPs obtained from harsher or milder treatments. Thus, only samples prepared below 260 °C were considered for the further discussion on the general properties of TSCP. Additionally, a considerable sulfur content was determined in all TSCP samples from H_2SO_4-treated MCC (Tables S6 and S7). It decreased with increasing temperature and treatment time, presumably due to expulsion of H_2SO_4 or SO_3. This offers another explanation for the slight decrease in isolable material over time. The sulfur values were used to calculate the residual H_2SO_4 content of the TSCP samples, which reached from 5.2 wt% for the mildest treatment to 0.6 wt% after treatment for 6 h at 250 °C. The reported elemental compositions were corrected with the calculated H_2SO_4 content. However, it is likely that the treatment also leads to partial modification of the intermediates, *e.g.*, *via* sulfate half esters. This would influence the correction and was indicated by the unchanged sulfur contents determined after purification of selected TSCPs *via* dialysis against H_2O for several days (Table S6). The possible correction bias would have a pronounced influence only on the values with higher sulfur contents of samples prepared under milder conditions, where the presence of free H_2SO_4 is more likely according to the steady decrease of its content over time.

Additionally, the influence of $(NH_4)_2HPO_4$ and ammonium *p*-toluene sulfonate – two similarly applied dehydration catalysts used in cellulose fiber carbonization [78] – was investigated. Only preliminary screenings by isothermal treatments at 250 °C were conducted. The observed behavior was similar as for the H_2SO_4-treated samples (Figure S18), and a plateau value was reached already at the beginning of the treatment. The formation of a stable intermediate was confirmed by elemental analysis and FTIR (Table S8 and Figure S28). However, when comparing the FTIR spectra of the TSCP intermediates obtained with different dehydration catalysts, clear differences were discernible (Figure S29). While the key vibrations corresponding to carbonyl, carboxyl and alkene moieties were similar, the absorptions in the area of 900–1300 cm^{-1} did not align. Given that ammonium salts and rather high catalyst loadings were used we assume that liberated ammonia participated in the transformations and altered the course of chemical reactions, *e.g.*, *via* Maillard intermediates. This was indicated by nitrogen contents of around 1 % in the isolated TSCP materials which did not decrease over prolonged heat treatment (Table S8). Moreover, the higher boiling points of phosphoric acid and *p*-toluene sulfonic acid prevent a facile removal of the catalysts. Nonetheless, we postulate that the major action of all applied dehydration agents is similar and relies on the strong acidities and water withdrawing properties of the employed reagents. This effect occurs directly in the case of H_2SO_4 or after expulsion of ammonia by high temperature treatment and liberation of the associated strong acids in the case of $(NH_4)_2HPO_4$ and ammonium *p*-toluene sulfonate.

Overall, the thermal analysis, elemental analysis and FTIR prescreening showed that a pure and thermally stable first carbonization intermediate can be prepared by sufficient isothermal treatments. The chemical composition remained unaltered, in line with the stabilization of the weight loss behavior. The process can be accelerated significantly by addition of dehydration catalysts. Different analytical markers were sufficient to detect potential residual cellulose contaminations in the samples. If preparation of a model TSCP material is anticipated, we

suggest monitoring for a constant weight over time during preparation (± 1–2 wt%) in connection with constant elemental compositions, and absence of cellulose resonances in the FTIR (Fig. 4) or solid state ^{13}C NMR spectra (Fig. 5). In TGA experiments pure TSCP materials resulted in char yields close to 50 % at 1500 °C (Table 2) and residual cellulose led to decreased char yields in connection with a shoulder in the DTG plots around 300 °C (heating rate of 10 K min^{-1}). Overall, the use of H_2SO_4 as catalyst is recommended. Insignificant amounts of heteroatoms were incorporated into the TSCP using H_2SO_4. Moreover, the sulfur content can be reduced to below 0.5 wt% upon sufficient isothermal treatments (Table S6), and complete removal during subsequent carbonization was reported [30]. To prevent unwanted follow-up reactions which were discernible when working with **MCC_SA-2** and at higher temperatures, an excessive catalyst loading and temperatures above 250 °C should be avoided. The occurrence of follow-up carbonization reactions can be spotted in an increase of the carbon content or slight shifts in the van Krevelen diagram (Figure S25). While it was not investigated in this study, it seems probable that lower H_2SO_4 contents will be sufficient for the isothermal preparation of TSCP and will reduce potential follow-up reactions during preparation.

3.2. Characterization of TSCP and comparison with hydrochars and humins

3.2.1. Preparation of hydrochars and comparable materials from literature

A comparative analysis was conducted to investigate the hypothesis that the isolated thermostable condensed phase can be characterized as a polyfuranic material and shows similarities to hydrothermally prepared humins. The results of our TSCP analyses were compared with those of hydrochars prepared directly from MCC and with literature reports (Table S3) [68,72,73]. Three different kinds of hydrochars were obtained at 220 °C, by adjusting the pH during hydrothermal treatment from acidic (added H_2SO_4) over neutral (H_2O only) to alkaline (added KOH). In conducted pre-screenings the hydrochar obtained under alkaline conditions did not show similarities with the TSCP samples prepared under neutral or acidic conditions. It was thus excluded from the further discussion. An influence of the pH on the formed structures was also described for humins derived from glucose [72]. The addition of H_2SO_4 accelerated the conversion under hydrothermal conditions and a hydrochar free from cellulose starting material was obtained already after 4 hours. Complete transformation under neutral conditions was only achieved after 8 hours. The analytical data of samples obtained after 2 and 4 hours respectively showed similarities to the not completely thermostabilized TSCP samples observed without addition of dehydration catalyst at temperatures below 270 °C (Figures S17 and S30). Characteristics of differently prepared cellulose based hydrochars were reported earlier [68]. Thus, only a few selected materials were prepared, and their characterization results were in line with literature reports. Samples **HC_W_8h** and **HC_SA_4h** were used for comparison, representing completely transformed hydrochars prepared under neutral and acidic conditions.

The similarities of the formed structures were confirmed on basis of their elemental compositions, SEM images, and the FTIR and solid state ^{13}C NMR spectra. The elemental compositions and spectroscopic data were compared with literature reports obtained for humins prepared from monosaccharides [73]. The chemical model structure for a humin used in the further discussion was also extracted from a study using milder conditions and ^{13}C labelled glucose as starting material [72]. We acknowledge that it was critically discussed in literature if the heterogenous hydrothermal carbonization of cellulose follows the same reaction mechanism as for the hydrothermal conversion of soluble monosaccharides. For example, Falco *et. al.* proposed a different behavior for hydrothermal cellulose conversion [67], rather following a mechanism similar to the one operative during dry pyrolysis. This would represent a conundrum in case the dry pyrolysis follows a mechanism that also incorporates a polyfuranic substance [74]. Moreover, in the same paper it was noted that the spectroscopic data obtained for materials of hydrothermal treatment of cellulose and glucose is practically identical if temperatures above 200 °C are used during the reaction. This suggests at least a common intermediate in both glucose and cellulose hydrothermal treatment [67]. The often-observed differences between humins and hydrochars are postulated based on the incorporation of aryl moieties into the structure [67,69]. A formation caused by subsequent follow-up reactions of a common polyfuranic intermediate is also conceivable. The latter is caused by the usually harsher conditions applied during the conversion of the more reluctantly reacting cellulose. We are aware that these known differences between the materials chosen for comparison will lead to some intrinsic shortcomings in the following discussion. However, the differences between humins and hydrochars in the solid state ^{13}C NMR spectra, which represent the main source to differentiate the materials, appear overall minor to us [67]. Especially when compared to spectra of cellulose carbonized at temperatures above ~ 350 °C [38,39,42]. The aim of this section is not to claim that humins, hydrochars and TSCPs are strictly the same materials, but to highlight similarities in their overall chemical composition.

3.2.2. Appearance and morphology

Irrespective of the complete conversion of all cellulose constituents, both the isolated TSCP samples and hydrochars were obtained as dark brown to black powders. However, the hydrochars had a feeble appearance and were visually less dense than the TSCP samples, which became evident when weighing in similar amounts of the respective materials for different analyses. SEM images revealed clear differences in morphology. While pure MCC exhibited a dense fiber-like structure, the hydrochars showed a porous and weakly-interconnected surface with microscale spherical welded-like particles. This is a known feature of cellulosic hydrochars and was ascribed to reactions and rearrangements following a nucleation and growth mechanism at the solid – liquid interface [67,69]. By contrast, the TSCP samples obtained under dry carbonization – both with and without dehydration catalysts – showed a smooth surface with no discernible differences to the MCC starting material (Fig. 6).

3.2.3. FTIR spectroscopy

The FTIR spectra of **HC_W_8h** and **HC_SA_4h** did not show significant differences. Key vibrations were visible around 1700, 1600, 1020, 800 and 765 cm^{-1} and a broad absorption between 1500 and 1100 cm^{-1} was observed. Representative TSCP samples prepared with and without H_2SO_4 as dehydration catalyst showed peaks in the same spectral areas. However, the peaks showed different appearances and proportions (Fig. 7). For example, the resonances at 1600 and 1700 cm^{-1} were broader and slightly shifted in the TSCP samples. A clear difference was discernible in the area between 1500 and 1020 cm^{-1} where the relative absorbance of the TSCP samples was weaker. Minor differences were also spotted in the shoulder around 950 cm^{-1} and for the peaks at 800 and 765 cm^{-1}. The TSCP obtained by addition of H_2SO_4 showed more similarities with the hydrochars than the TSCP of pure cellulose (Fig. 7).

A comparison of the spectra with FTIR data reported for humins prepared from different monosaccharides (glucose, fructose) shows clear similarities in the characteristic vibrations. The signal around 1700 cm^{-1} was assigned to C═O stretching of carbonyl and carboxyl functionalities [73]. The peaks at 1600 and 1020 cm^{-1} for the respective C═C and C-O stretches were ascribed to substituted furan rings. The signals at 800 and 765 cm^{-1} assigned to furan C-H out of plane deformation were detected in both hydrochars, but less pronounced in the TSCP samples. Differences in the spectral area of 1500–1020 cm^{-1} as observed between hydrochars and TSCP were also noted in fructose and glucose derived humins and ascribed to different proportions of 5-HMF incorporated into the polyfuranic structure [65]. In the case of TSCP prepared with H_2SO_4 also differences caused by the incorporation of sulfate half esters are feasible. However, we were not able to assign a prominent peak to this modification in any of the prepared samples.

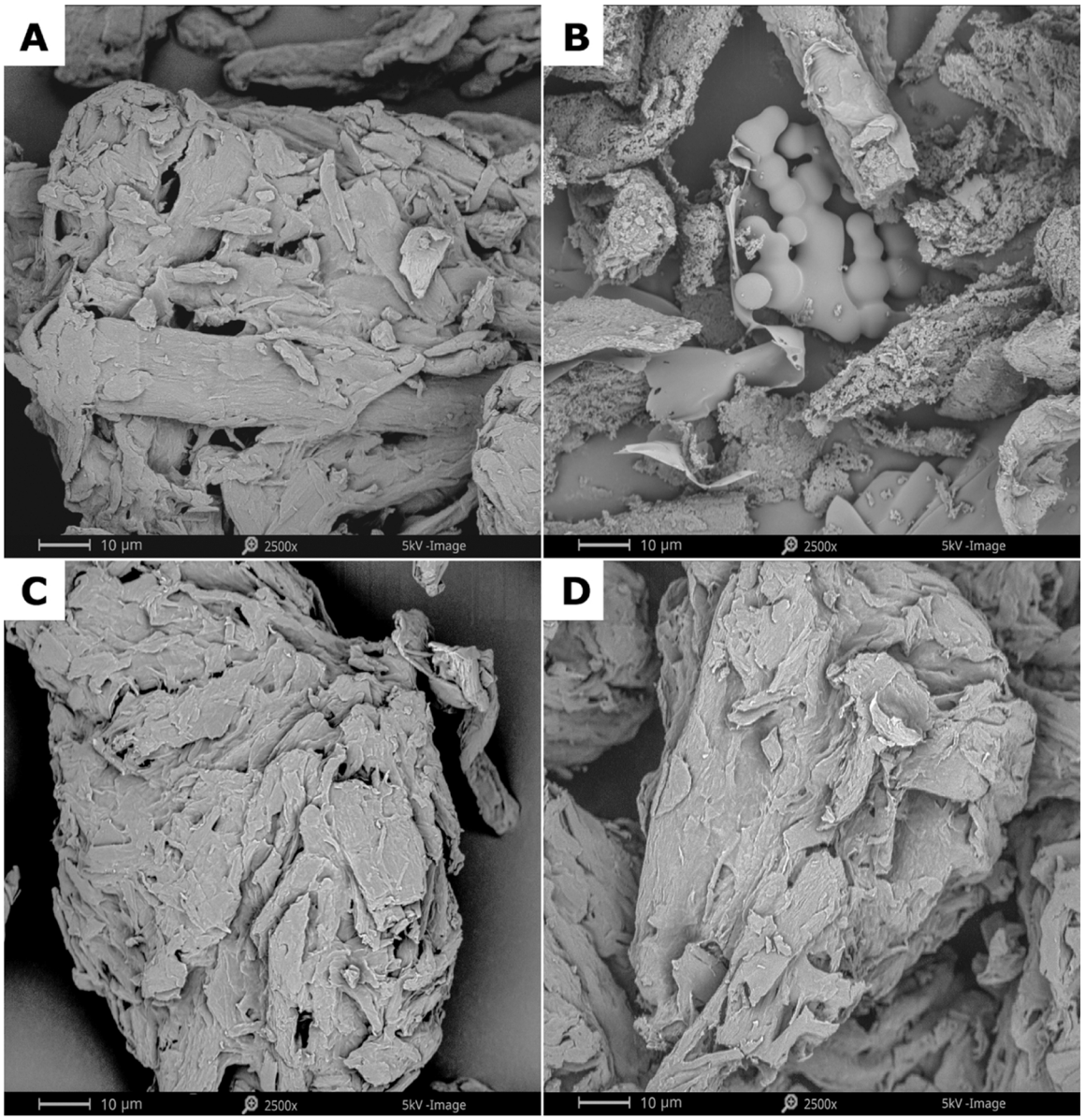

Fig. 6. SEM images recorded for representative hydrochars and TSCP intermediates prepared in this study. **A**) untreated MCC starting material; B) HC_SA_4h; C) TSCP_SA_250_6h; D) TSCP_P_270_12h. Scale bar = 10 µm.

3.2.4. Solid state ^{13}C NMR spectroscopy

In the solid state ^{13}C NMR spectra subtle differences between **HC_W_8h** and **HC_SA_4h** were visible. The sample prepared without addition of acid catalyst showed minor signals of unreacted cellulose (sharp peaks at 70 ppm). Additionally, a shoulder in the aromatic region at 130 ppm was present, presumably caused by benzylic structures. The spectrum of the hydrochar prepared under acidic conditions showed very similar peaks as reported for glucose derived humins [67,73]. Several signals characteristic for a polyfuranic network were present and could be assigned (dashed lines in Fig. 8) [73].

In line with the FTIR analysis, the ^{13}C NMR spectra demonstrated clear similarities between the hydrochars and TSCP samples. All investigated materials showed peaks assignable to a polyfuranic network. However, the differences between TSCP and hydrochar became more pronounced. The most characteristic difference for both TSCP samples was apparent between 90 and 50 ppm with a strong and broad peak partly overlapping with the alkyl resonances. This suggests the presence of considerable amounts of alcohol or ether functionalities. The peak was stronger for the TSCP sample prepared without addition of dehydration catalyst. This can be explained by the incorporation of considerable fractions of only partly dehydrated saccharide structures in the case of dry pyrolysis. The spatial proximity of reactive dehydration intermediates might favor the incorporation of less reactive intermediates into the TSCP scaffold. Moreover, the inhomogeneous distribution of catalytically active H_2O or dehydration catalysts in the solid state can prevent a full conversion to 5-HMF moieties. We exclude the possibility that the signal can be ascribed to unreacted cellulose. The peak did not change in the temperature area of 200–250 °C in case of the TSCP materials prepared under H_2SO_4 catalysis (Fig. 5B). Additionally, prescreening using FTIR and thermal analyses did not indicate any residual cellulose. The maximum of the thermal degradation event was shifted to around 390 °C for the TSCP samples (Table 2; heating rate 10 K min^{-1}). This suggests the incorporation of saccharide moieties that cannot be removed over LGA volatilization with an expected maximum around 300 °C.

For the TSCP obtained without dehydration catalyst, also a pronounced shoulder at 130 ppm was visible. This can be ascribed to C=C bonds and due to follow-up reactions during the long treatment at 270

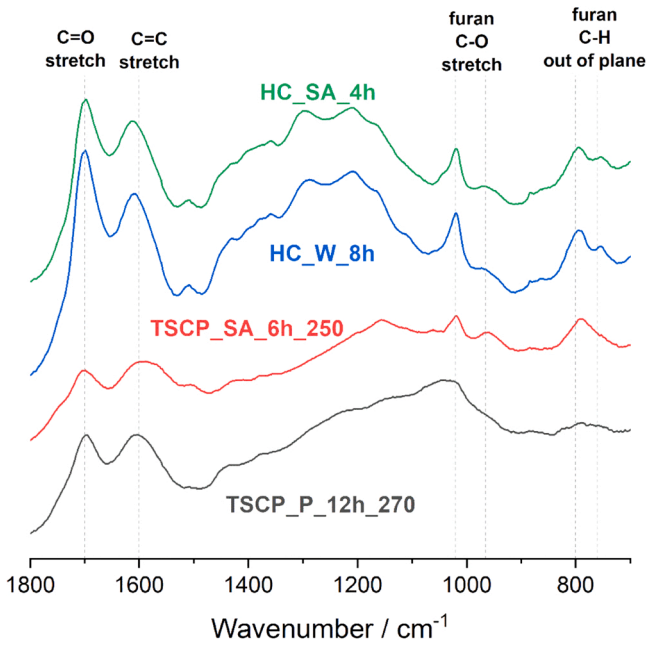

Fig. 7. Comparison of FTIR spectra obtained for selected cellulose free hydrochar and TSCP samples. Vibrations that were previously assigned to glucose based humins are highlighted with dashed lines [73].

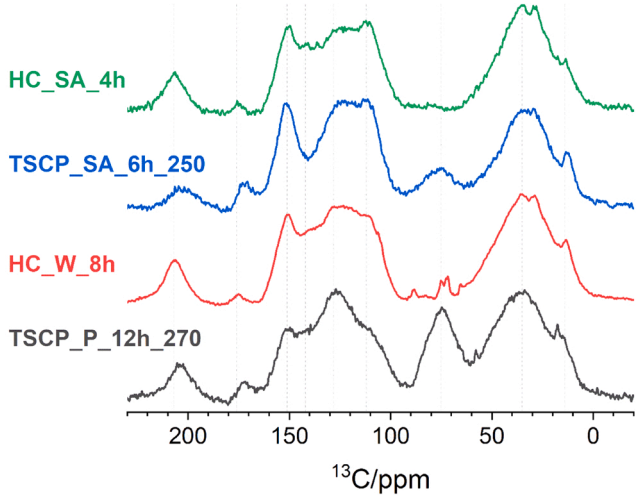

Fig. 8. Comparison of solid state ^{13}C NMR spectra obtained for selected cellulose free hydrochar and TSCP samples. Signals that were previously assigned to glucose based humins are highlighted with dashed lines [73].

°C leading to the minor formation of benzylic structures. Such shoulders were also observed in cellulose hydrochars prepared using harsher conditions [67,69]. Nonetheless, the spectra did not align with data reported for cellulose chars obtained at temperatures above 300 °C, which showed a considerably stronger further conversion [38,39]. In the H_2SO_4-treated TSCP samples a slightly stronger resonance around 180 ppm for carboxylic groups and a characteristic "tent" in the aromatic region around 140 ppm was observed. The slight increase in the carboxylic content might be caused by the oxidative nature of the H_2SO_4 catalyst. A peak at 142 ppm was previously assigned to α-carbons of terminal furans [73]. This suggests differences in the formed bonds in the polyfuranic network caused by the catalyst.

3.2.5. Elemental composition and dehydration behavior

The chemical compositions determined by elemental analysis were compared with literature reports for both MCC derived hydrochars and monosaccharide based humins [68,73]. The similarities in the dehydration behavior during dry pyrolysis in the **TSCP_P** series and hydrothermal treatment were plotted in a van Krevelen diagram (Fig. 9A). Values reported by Paksung *et al.* for hydrochars prepared from MCC without addition of catalyst are included for comparison [68]. With increasing treatment intensity (time, temperature) the material gradually dehydrates until the cellulose is completely transformed to a dehydrated intermediate (*i.e.*, hydrochar or TSCP). The chemical composition of the intermediate does not change considerably if the treatment is continued. A major difference can be spotted in the kinetics of the transformation. During hydrothermal treatment only 30 or 45 minutes at 240 °C were necessary to reach an almost stable chemical composition, while under dry conditions at least more than 6 hours at 270 °C were required.

To showcase the similarity with other polyfuranic substances, the elemental compositions of all completely transformed TSCPs, in which no follow-up reactions were indicated, were plotted against the values for cellulose based hydrochars [68] and humins derived from different monosaccharides [73] (Fig. 9B). While there were small differences in the positions of the clusters of the differently prepared materials, all datapoints appeared at values characteristic of polyfurans.

3.2.6. Thermal analysis and gas evolution

Lastly the thermal degradation and the associated gas evolution of the isolated TSCP materials and hydrochars was examined by STA-MS experiments. Two sets of experiments were conducted on the same materials with different devices. In the first the CO, CO_2, H_2O, CH_3 and H_2 evolution at a heating rate of 10 K min^{-1} was monitored according to a previous report on humin pyrolysis (Fig. 10) [70]. In the second set a quantitative evaluation of CO, CO_2 and H_2O as the major analytes associated with char formation was attempted also using a heating rate of 10 K min^{-1} (Table 2) [81].

Despite the differences between TSCPs and hydrochars in their chemical composition, all materials without cellulose contamination resulted in char yields in a narrow window between 47 and 50 wt% at 1500 °C (Table 2). The DTG maxima were determined on two separate devices and appeared in a broad peak between 410 and 430 °C for the hydrochars, between 400 and 420 °C for the TSCPs prepared with H_2SO_4 catalyst and between 375 and 390 °C for the TSCPs prepared without catalyst (Table 2 and Table S10). The earlier onset of thermal degradation in TSCP is ascribed to the presence of the less thermally stable alcohol and ether functionalities, which disintegrate rapidly at temperatures over 350 °C. Expulsion of CH_3 was only observed in these samples and indicated the occurrence of fragmentation reactions (Fig. 10D). This can also explain the higher mass change at the DTG maximum observed for **TSCP_P**, whereas the determined values for the **HC** and **TSCP_SA** materials were almost identical (Table 2).

During gas monitoring (Fig. 10) the hydrochars showed a very similar profile as reported for a glucose based humin, with a broad expulsion of analytes between 300 and 1000 °C [70]. The first thermal event associated with the disintegration of the polyfuranic network can be observed around 400 °C connected to the expulsion of H_2O, CO and CO_2. A second skewed maximum occurs for CO_2 between 550 and 600 °C, while both CO and H_2O get removed in a separate event occurring around 700 °C. Both can be associated with the disintegration of yet unknown subsequently formed carbonization intermediates. The apparent increase in CO expulsion at temperatures approaching 1000 °C is an artifact from baseline correction and does not correspond to a further transformation. Additionally, weak formation of CH_3 and H_2 with broad peaks and maxima around 550 and 750 °C were observed. These can be associated with homolytic fragmentation reactions or the fusion of benzene rings.

Despite the overall similar thermal behavior of the hydrochars and TSCPs (Table 2) which indicates similarities in the operative pyrolysis reactions, differences in the released gas of the TSCP samples was

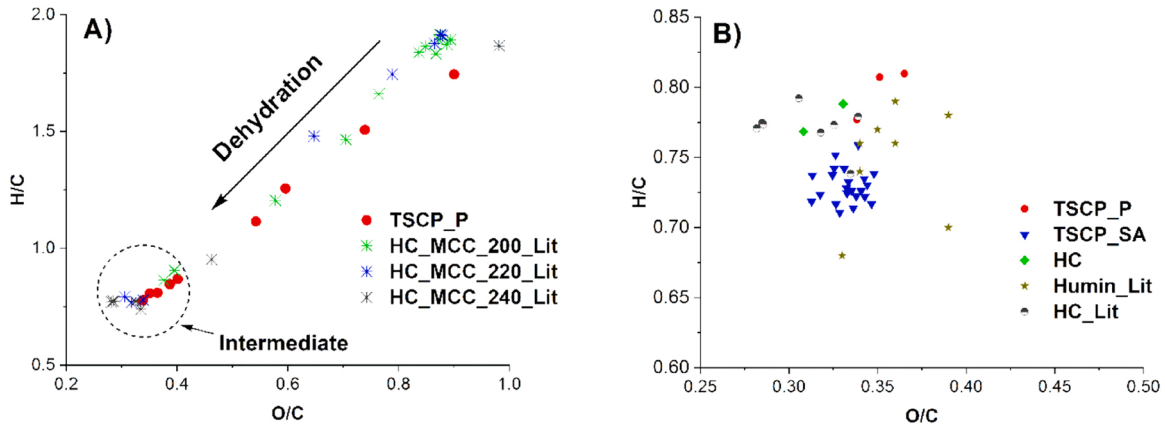

Fig. 9. Van Krevelen diagrams comparing: A) The dehydration behavior in the TSCP_P series with literature values reported for the preparation of MCC based hydrochars [68]. Both show a release of H_2O with increased treatment time and temperature, until an intermediate is reached, and the chemical composition stays almost constant. B) The elemental composition of TSCPs and HCs prepared in this study with literature values reported for MCC based hydrochars [68] and monosaccharide based humins [73].

observed. The CH_3 and H_2 expulsion profiles were similar, but the peaks for H_2O, CO and CO_2 did not align. Clearly separate thermal events were not apparent in the TSCP samples. While this issue needs further investigation, we must stress analytical limitations caused by the composition of the TSCP materials. *E.g.*, in a reproducibility test conducted for **TSCP_SA_200_6h** the overall thermal behavior (DTG, TGA) was almost identical, but the peaks and maxima of the individually monitored gases showed slightly shifted maxima and appearances (Figure S31). The initial strong disintegration of the incorporated partly dehydrated structures resulted in peak superpositions. This issue was especially severe in the **TSCP_P** materials (Fig. 10D). For all **TSCP_SA** materials the H_2O peak was very broad over the whole investigated temperature area (Fig. 10C). This might relate to the hygroscopic nature of residual sulfuric acid or sulfate half ester groups. Carbonization up to 1000 °C is also associated with the volatilization of other low molecular weight compounds, which was not examined in this study.

Additionally, it was attempted to quantify the evolved H_2O, CO and CO_2 up to 1500 °C [81], as the volatiles most commonly associated with char formation. Insights can be gained from the ratio in which they are formed. For the hydrochars, a ratio of approximately 4:2:1 (H_2O: CO: CO_2) was observed, while it was around 4:3:1 for the **TSCP_P** materials. As expected from the higher carboxylic acid content observed in the solid-state NMR spectra, the **TSCP_SA** series exhibited a higher CO_2 evolution. The relative CO expulsion for the **TSCP_SA** samples obtained below 230 °C was higher than for the samples prepared at higher temperatures. Although no considerable differences in the chemical composition were apparent (Fig. 5), there were differences in the H_2O expulsion at temperatures above 500 °C (Figure S34). It is yet unclear if this is related to supramolecular rearrangements or represents an artifact from the higher H_2SO_4 contents determined in the samples obtained at lower temperatures (Table S6).

3.3. Implications for the reactions during cellulose dehydration

3.3.1. Comparison of thermal TSCP and humin formation

The data presented in the previous section showcased the clear similarities between the chemical composition of intermediate TSCP materials obtained during dry pyrolysis of cellulose with cellulosic hydrochars obtained *via* hydrothermal conversion. Furthermore, the gathered data aligned with reports on glucose derived humins [72,73]. While we by no means intent to claim that the operative transformations are strictly identical – which was for example evident in the differences in the morphology or the incorporation of alcohol and ether functionalities in the NMR spectra – we believe that the presented data is sufficient to characterize the obtainable TSCP intermediates as a polyfuranic substance. This means that the initial reactions during the char forming pathway in cellulose dry pyrolysis are similar to the reactions operative during the hydrothermal carbonization of other saccharides or the general carbonization of sugars [7]. The initial and yield determining step in the dehydration of cellulose is the polycondensation of generated 5-HMF structures and other reactive saccharidic dehydration intermediates to a polyfuranic network. Based on mechanistic considerations, 5-HMF structures can only derive from REGs, liberated glucose units or LGA moieties. Thus, depolymerization reactions must be important also during the initial carbonization reactions – and not only in the volatilization pathway. The clear isolation of TSCP as first carbonization intermediate further contradicts prevailing mechanistic proposals for char formation favoring direct dehydration of the glycopyranose units [41] or reactions on the non-reducing ends [23]. Instead, the benzene moieties in the ultimate carbon network must evolve through the transformations of furans – as proposed by Pastorova et al. [39].

Besides the initial report on TSCP [39], the findings of this study are in line with the mechanistic proposals of Kawamoto and his coworkers [51,55–57,74]. Their work highlights the importance of REG, LGA and 5-HMF structures during cellulose carbonization [56,57,74]. With the isolation and thorough characterization of pure TSCP at hand, we can support the overall mechanistic proposals of Kawamoto's group for initial cellulose dehydration and want to expand and refine it in some parts. Noteworthy, the following transformations and structures are for "slow" pyrolysis of cellulose, *i.e.*, under conditions that favor char formation and are for example used in cellulosic carbon fiber production. There might also be some similarities to the charring side reactions observed during "flash pyrolysis" conditions, *i.e.*, when the production of LGA or other volatiles are anticipated [76]. However, as the operative rapid heating rates to temperatures beyond 400 °C also allow for direct elimination of H_2O from the cellulose backbone and will favor fragmentation reactions, the underlying mechanism might be considerably different.

3.3.2. Dehydration and formation of TSCP

It is postulated that the initial dehydration reactions responsible for charring reactions below 300 °C occur selectively on the reducing chain ends of cellulose (Scheme 1). Two pathways for the formation of 5-HMF structures due to loss of H_2O from end group pyranoses seem conceivable. Either involving the dehydration of LGA-terminated structures [52] to levoglucosenone (LGO) and subsequent rearrangement [83,84], or the dehydration of REGs over different enolizable and cyclic intermediates [49,51]. The lower thermal stability of monosaccharides compared to LGA suggests that REGs are more susceptible towards

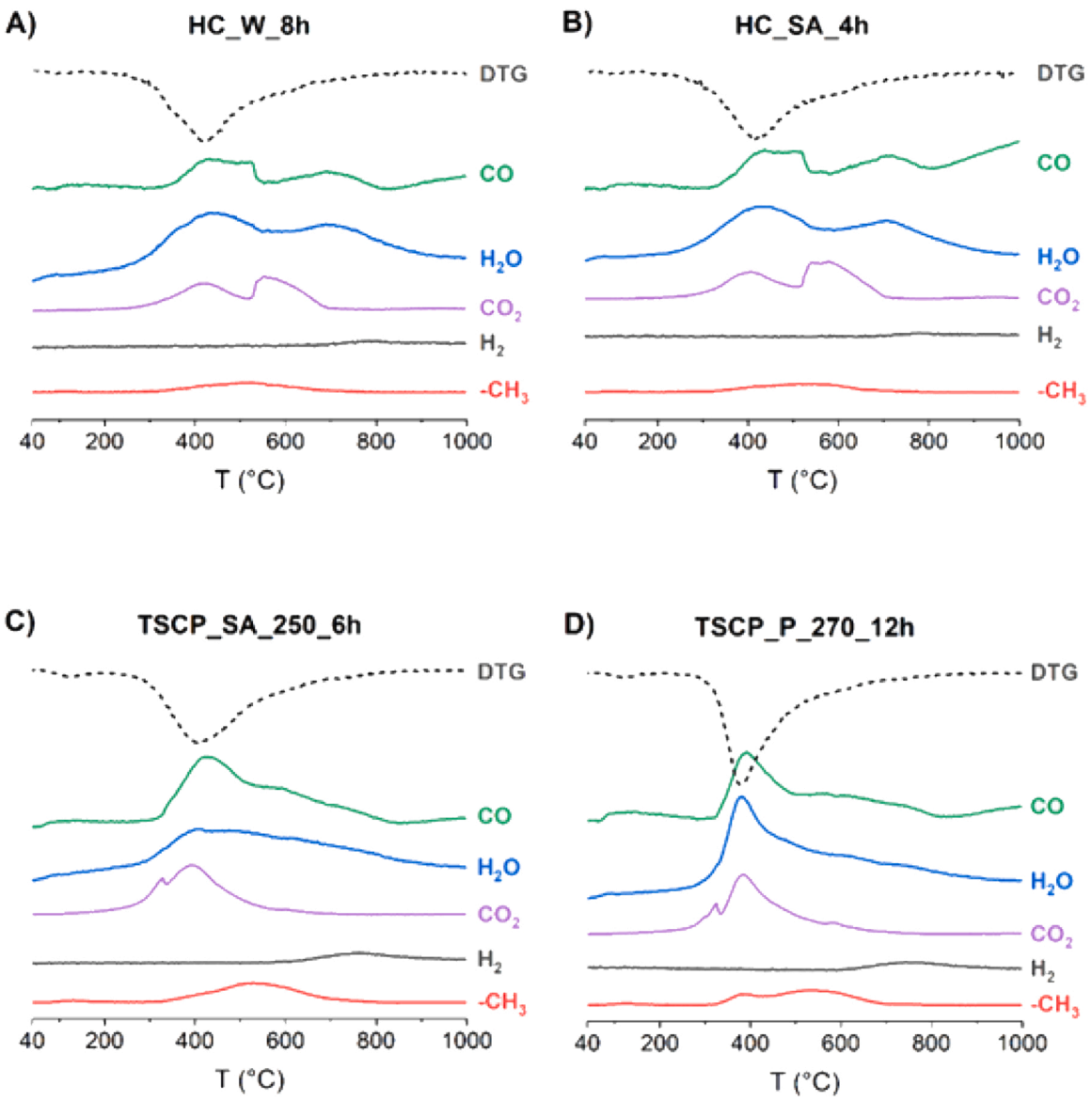

Fig. 10. Comparison of the evolved gaseous products during thermal treatment for representative hydrochars (A and B) and TSCPs (C and D) prepared in this study. DTG-MS plots for continuous heating under 70 mL/min He flow from 40 to 1000 °C at a heating rate of 10 K min^{-1}. Selected ions for MS: 2 amu (H_2), 15 amu (CH_3), 18 amu (H_2O), 28 amu (CO) and 44 amu (CO_2). Note that the increase in the CO expulsion towards 1000 °C represents an artifact from baseline correction.

Table 2
Values for char yield and DTG peaks obtained for the thermal analysis of different polyfuranic substances prepared in this study. A quantitative evaluation of the expulsed gases was conducted for H_2O, CO and CO_2 [81].

Sample	Char[a] / wt%	DTG peak[b]		Evolved gas / mmol g^{-1}			Relative to H_2O		
		°C	% min^{-1}	H_2O	CO	CO_2	H_2O	CO	CO_2
HC_SA_4h	49.3	429.4	-2.1	0.75	0.36	0.19	1.0	0.48	0.25
HC_W_8h	48.4	422.4	-2.3	0.83	0.40	0.21	1.0	0.48	0.25
TSCP_P_12h_270	47.9	385.1	-3.3	0.68	0.51	0.17	1.0	0.75	0.25
TSCP_P_12h_280	49.6	390.1	-3.1	0.62	0.50	0.15	1.0	0.81	0.24
TSCP_SA_6h_210	48.2	419.2	-2.1	0.70	0.79	0.30	1.0	1.13	0.43
TSCP_SA_6h_220	48.5	415.8	-2.1	0.44	0.57	0.20	1.0	1.30	0.45
TSCP_SA_6h_230	46.6	412.2	-2.1	0.74	0.54	0.31	1.0	0.73	0.42
TSCP_SA_6h_240	47.2	418.6	-2.2	0.74	0.56	0.31	1.0	0.76	0.42
TSCP_SA_6h_250	47.4	410.4	-2.2	0.71	0.52	0.29	1.0	0.73	0.41

[a] residual solid in the TGA measurement at 1500 °C
[b] heating rate 10 K min-1

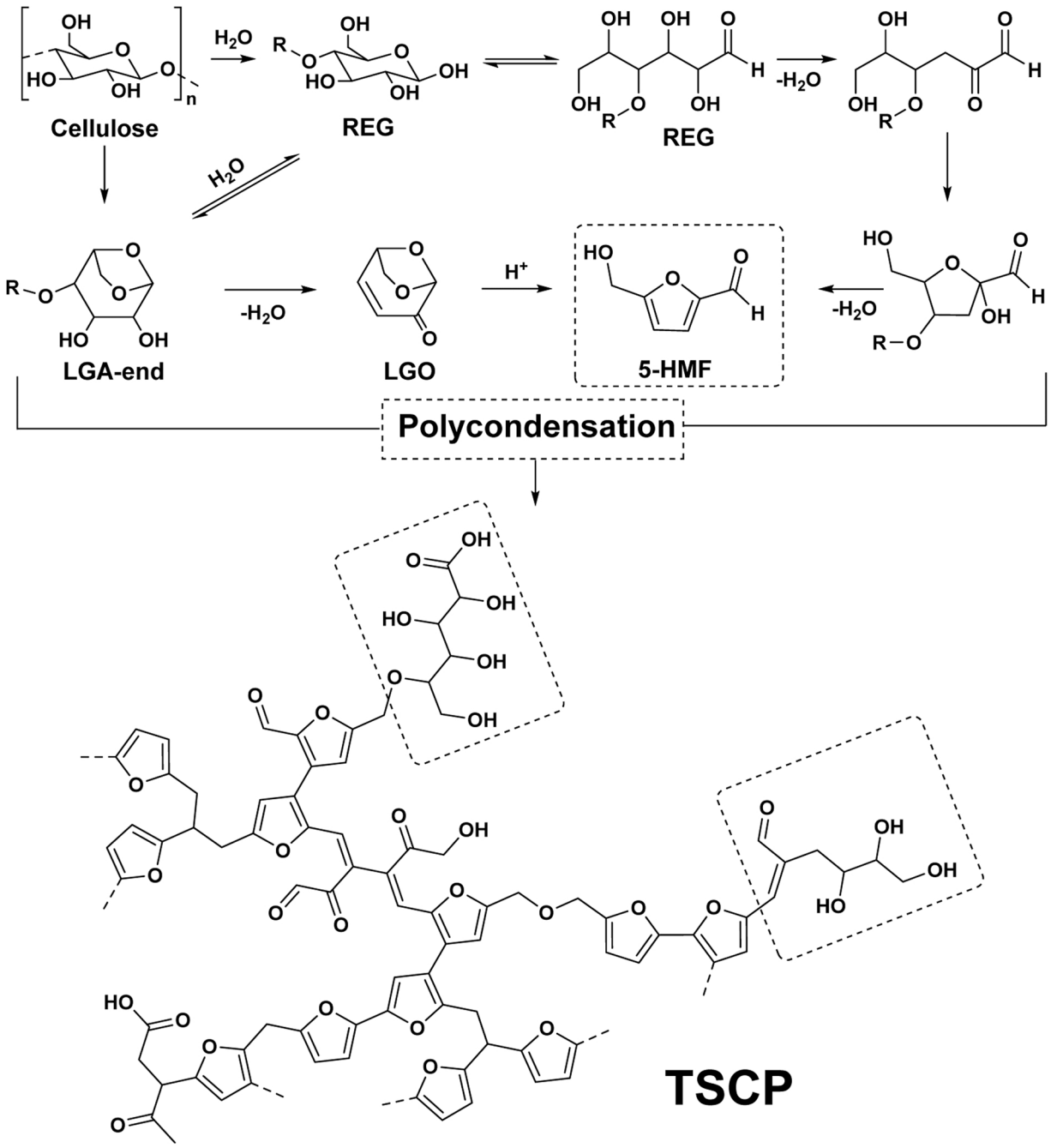

Scheme 1. Proposed dehydration reactions operative in the carbonization pathway during slow pyrolysis of cellulose. It is postulated that the LGA or REG moieties serve as source for the removal of water either over rearrangements or a mechanism involving energetically favored enol and cyclic intermediates [51]. New REGs are gradually produced during the process due to hydrolysis of glycosidic bonds through generated H_2O. 5-HMF and partly dehydrated, reactive structures undergo a polycondensation resulting in TSCP as first intermediate in the carbonization sequence. The postulated structure for a representative fragment of TSCP was adapted from a proposal for a glucose-based humin [72] by incorporation of partly dehydrated saccharide moieties (dashed boxes).

dehydration at the operative temperatures of 200 – 300 °C. Once the initial dehydration occurred, the liberated H_2O can hydrolyze further glycosidic bonds or LGA moieties. This results in the liberation of REGs which are more susceptible to dehydration causing an autocatalytic reaction progress as proposed by Kawamoto et al. [56,74] The dehydration is strongly accelerated by the addition of acids (Fig. 3). During carbonization of pure cellulose, a catalytic effect of generated acidic light oxygenates (*i.e.*, carboxylic acids) on the overall reaction progress is conceivable [23]. Such compounds are often observed as side products during hydrothermal 5-HMF production [85,86], or might be formed during fragmentation reactions of cellulose [51]. The obtainable yields for TSCP (Fig. 3) were considerably lower than the theoretically expected value of 66.6 % for the transition of cellulose ($C_6H_{10}O_5$) to a hypothetic, ideal humin structure only consisting of condensed 5-HMF structures ($C_6H_4O_2$). Consequently, additional formation of volatiles (*i.e.*, removal of tar fractions or light oxygenates) must superimpose the initial dehydration even when using conditions strongly favoring char formation.

The presence of alcohol or ether moieties in the ^{13}C NMR spectra of isolated TSCPs suggests the incorporation of only partly dehydrated saccharides into the intermediate, especially when no catalyst was added. This represents the biggest determined difference in the chemical

composition of hydrochars and TSCP. How these saccharidic structures are incorporated into the structure could not be determined with the analytical techniques available in this study. However, we suggest that they derive from cellulose monomers or REG dehydration intermediates [51], which underwent a stable chemical modification that inhibits further enolization or cyclization reactions. Thereby, the release of H_2O from the saccharidic structures or their removal over LGA formation is prevented below 300 °C. As the mechanisms of humin formation are still debated in literature [62–66], we refrain from further speculation on other differences stemming from the dry pyrolysis conditions.

Scheme 1 shows the proposed structure of TSCP. It is based on a model described for a glucose-derived humin [72], modified with partly dehydrated saccharide structures. It is noteworthy that different structural models were postulated for saccharide based humins [70,71,73]. While we are optimistic that Scheme 1 displays the main functional groups present in TSCP, it represents only a first approximation based on the current knowledge. More sophisticated analytical techniques (*i.e.*, 2D solid state NMR [38,72]) will be needed to refine our proposal and obtain a better understanding of its connectivity. In the TSCP samples isolated at higher temperatures (> 250 °C) the formation of minor amounts of benzene moieties was also indicated in the performed analytics. However, they were not included in the structural model. We interpret their presence as a consequence of first carbonization follow-up reactions in TSCP caused by the harsher preparation conditions. It is postulated that they are not formed in significant amounts during the initial dehydration and polycondensation reactions.

3.4. Implications for the further carbonization sequence

In the extensive literature on cellulose pyrolysis, it is generally agreed on that the formation of the fused carbon network in the chars is associated with the generation of H_2O, CO and CO_2. However, surprisingly little information or even speculations are available on the chemical transformations or structures involved in the formation of the observed products [41]. Similarly, there are only limited structural schemes in the reports focusing on humin or hydrochar pyrolysis [70, 87]. Based on the isolation of a polyfuranic TSCP as a first carbonization intermediate and the obtained STA-MS results (Fig. 10) we want to highlight certain observations and outline conceivable reactions occurring in the further carbonization steps. We acknowledge that the following discussion will rely on preliminary data and is in parts speculative. It should not be seen as a definite mechanistic proposal that incorporates all reactions during char formation but as a starting point for further scientific discussion.

3.4.1. Gas evolution during carbonization

While issues due to partial peak overlap in the MS monitoring were encountered during the thermal analysis of the TSCP materials, it was possible to observe different events associated with gas evolution in the further carbonization sequence up to 1500 °C. This was achieved through the conducted independent thermal analysis of the isolated carbonization intermediate. The usually occurring dominating peak caused by the analytes stemming from the cellulose volatilization pathway (*i.e.*, LGA evaporation and associated side reactions) could be avoided (compare Fig. 10 and Figure S3). In accordance with literature reports on humin pyrolysis, the observed evolution of H_2O, CO, CO_2, CH_3 and H_2 from the different polyfuranic substances between 300 °C and 1000 °C investigated in this study was not summarized in one definite temperature region [70]. In the case of CO_2 and H_2O they appeared almost bimodal for some samples and did not occur concomitantly with the CH_3 or H_2 maxima. Overall, this suggests the occurrence of different intermediates and independent reactions in the temperature range of 300 – 1000 °C. While we postulate that the reactions leading to the initial H_2O, CO and CO_2 evolution from TSCP up-to a temperature of approximately 400 °C (Fig. 2) are primarily governed by heterolytic processes, the observed expulsion of CH_3 and H_2 indicated the presence of homolytic bond cleavages and associated radical reactions. It seems likely that this more complex processes start to dominate the reactions in the temperature area above ~ 500 °C.

As described above, a major part of the overall H_2O expulsion observed during cellulose carbonization can be ascribed to the initial dehydration and polycondensation reactions. Formation of CO and CO_2 below 300 °C was minor and probably connected to different not further examined side reactions. Based on the solid state ^{13}C NMR spectra (Fig. 8) and the postulated structure of TSCP (Scheme 1) the chemical moieties serving as sources for the observed gases at higher temperatures can be postulated. The expulsion of CO and CO_2 around 400 °C is likely connected to the respective carbonyl and carboxyl functionalities incorporated in the TSCP structure. The concomitantly appearing H_2O peak might relate to reactions leading to the first benzene structures. Comparing the monitored gas evolution from the TSCP materials and hydrochars, the signals in TSCP appeared more superimposed over the monitored temperature area. Moreover, TSCP prepared without dehydration catalyst had a considerably higher gas evolution at the early stages of the thermal degradation around 400 °C. We surmise both is a consequence of elimination and fragmentation reactions of alcohols and ethers stemming from incorporated partly dehydrated saccharidic structures resulting in H_2O, CO_2, CO and CH_3 expulsion (Fig. 10). They will also serve as a source for weight losses due to volatilization of light oxygenates. Potential reactions of the incorporated alkyl moieties are more difficult to outline. They are expected to be mostly present as linkers between furanic moieties [72] – or at higher temperatures benzylic structures [38]. From solid state NMR investigations, it can be surmised that they are more thermally stable than the alcohols, ethers, carbonyls, and carboxyl groups [LF_41,43,44]. Fragmentations and eliminations at higher temperatures seem likely, but we do not exclude the possibility of more complicated aromatic rearrangement reactions and incorporation into the carbon structure. Expulsion of H_2O, CO and CO_2 was also observed at temperatures over 400 °C where the structural features reminiscent to TSCP started to disappear [38,39,42]. Thus, a part of their overall evolution must be connected to moieties of not yet identified structures formed from the polyfuran network at temperatures above ~ 400 °C.

3.4.2. Reactions leading to the first benzylic intermediate

As discussed, a transition from the isolated TSCP directly to a polycondensed carbon network seems unlikely. The relatively high peak intensities of the benzene moieties in reported CP MAS solid state ^{13}C NMR studies [38,39,42] suggest the presence of less condensed benzylic intermediates up-to a temperature of around 800 °C [42]. The H_2 evolution monitored in our study showed a maximum in a similar temperature area (Fig. 10) and might relate to the fusion of the benzene rings. Based on elemental analysis results it is agreed on that oxygen is incorporated into the char structures after high temperature treatment (~ 1000 °C) [30,41,58]. This is associated with the presence of phenol moieties in the polyaromatic structures [87,88]. The speculations reported in literature on how phenol moieties might be formed from a polyfuran during the further carbonization sequence are limited and inconclusive. Based on pyrolysis GC/MS results Pastorova *et al.* postulated pathways leading directly from a furan to phenolic structures in their initial report on TSCP. These included retro-aldol reactions followed by rearrangements, or Diels Alder reactions of furan with reactive dienes formed due to fragmentation side reactions [39]. However, there are also reports favoring the incorporation of benzofuran structures in chars isolated between 300 – 400 °C [38,87,89]. This would suggest that phenols are primarily formed later in the carbonization sequence due to rearrangement reactions in initially formed benzylic intermediates. In a recent 2D HETCOR NMR study by Knicker *et al.* the structure of cellulose char obtained from MCC after inert pyrolysis at 350 °C for 1 h was discussed in detail [38]. Their data strongly suggested that the aryl moieties formed at these temperatures are primarily present as benzofuran and dibenzofuran structures in shorter fragments (Scheme 2).

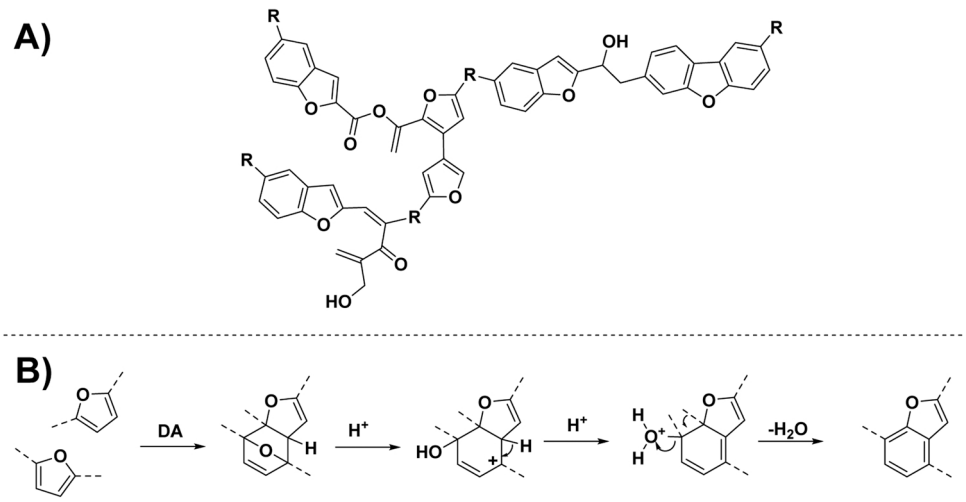

Scheme 2. A) Structural proposal for a fragment present in a cellulose char carbonized at 350 °C for 1 hour according to a 2D solid state HETCOR NMR study reported by Knicker et al. [38] B) Potential pathway for the conversion of furan moieties present in humins to the evidenced benzofuran moieties involving a tandem Diels Alder dehydration mechanism [90].

Phenol moieties were not observed in their sample. Moreover, they also discussed the incorporation of the alkyl moieties into the structure in detail. They concluded that the aliphatics are mostly present as linkers between different aryl moieties. A similar connectivity *via* alkane linkers is often postulated for the furan moieties in humins [72,73].

We want to highlight their thorough structural proposal, as it can be interpreted as a direct follow-up product from certain postulated polyfuran models [70–73], when considering the fusion of furan moieties *via* a tandem Diels Alder – dehydration reaction (Scheme 2) [90]. Similar reactions during carbonization were so far only discussed for furans with reactive intermediates formed *via* fragmentations [39]. Recently Diels Alder chemistry of furans received renewed attention in context of the valorization of bioderived monomeric species [90]. Thereby, benzofuran formation and associated coking was also reported as a major unwanted side reaction in transformations with non-activated dienophiles at temperatures below 450 °C [91–93]. These reports suggest that such furan-furan Diels Alder reactions should in principle be energetically accessible in the operative temperatures of 300 – 400 °C.

4. Conclusions and outlook

By prolonging isothermal phases and / or applying dehydration catalysts it was possible to completely transform cellulose to TSCP as its first postulated carbonization intermediate at temperatures between 200 and 280 °C [39]. The chemical stability and absence of significant further carbonization reactions was confirmed with isothermal TGA experiments and thorough analyses of the isolated materials. With the optimized treatment conditions determined in this study it was possible to isolate TSCP without cellulose residues. This allowed for clean FTIR and solid state ^{13}C NMR spectra, and STA-MS thermograms and mass spectra, that are otherwise suffering from signals arising from residual cellulose. Consequently, the initial cellulose carbonization intermediate could be analyzed in more detail than previously possible.

The conducted comparative analysis with cellulosic hydrochars and literature values reported for glucose derived humins confirm the polyfuranic nature of TSCP first postulated by Pastorova et al. [39]. Our findings support that the initial reactions in the carbonization mechanism of cellulose are governed by localized dehydration at the REGs and polycondensation of the generated 5-HMF motifs [74]. The operative chemistry must thus be similar as the reactions occurring during hydrothermal treatments of (poly)saccharides or the carbonization of other monosaccharides [7]. The isolation of a pure polyfuran as first carbonization intermediate substantiates previously postulated dehydration mechanisms, which lacked unambiguous analytical evidence for their proposals [7,39,56,74].

Differences in the chemical composition of differently prepared polyfurans were determined. Compared to hydrochars or humins, the structural analysis of TSCP suggested a preferential incorporation of only partly dehydrated carbohydrate moieties and a varying connectivity of the polyfuran networks. However, it was not possible to further elucidate these structural differences with the analytical techniques available in this study. Additional studies on these topics are planned, aiming for a yet more detailed understanding of the TSCP structure and its formation.

Based on the obtained STA-MS results also preliminary insights on the further carbonization sequence was obtained. We want to highlight that the separate investigation of TSCP eliminated peak superpositions caused by the usually dominating tar forming pathway. Thus, it was possible to observe several thermal events connected with gas evolution in the temperature between 300 and 1000 °C. This strongly suggests the formation of different, not yet determined intermediates in the subsequent carbonization sequence. Isolation and characterization of these intermediates might expand the understanding of the reactions leading from cellulose to biochar [88].

CRediT authorship contribution statement

Lukas Fliri: Writing – review & editing, Writing – original draft, Visualization, Validation, Methodology, Investigation, Formal analysis, Conceptualization. **Kseniia Dubivka:** Writing – review & editing, Visualization, Investigation, Formal analysis. **Dmitrii Rusakov:** Writing – review & editing, Visualization, Investigation, Formal analysis. **Alexander Volikov:** Investigation, Formal analysis. **Chamseddine Guizani:** Investigation, Formal analysis. **Sami Hietala:** Investigation, Formal analysis. **Svitlana Filonenko:** Writing – review & editing, Investigation, Formal analysis. **Michael Hummel:** Writing – review & editing, Supervision, Project administration, Funding acquisition.

Declaration of Competing Interest

The authors declare that they have no known competing financial interests or personal relationships that could have appeared to influence the work reported in this paper.

Data availability

Data will be made available on request.

Acknowledgment

The authors gratefully acknowledge funding from the Research Council of Finland (former Academy of Finland; project number: 348354). The authors thank Muhammad Awais for help in the visualization of the results.

Appendix A. Supporting information

Supplementary data associated with this article can be found in the online version at doi:10.1016/j.jaap.2024.106591.

References

[1] M.J. Antal, M. Gronli, The art, science, and technology of charcoal production, Ind. Eng. Chem. Res. 42 (8) (2003) 1619–1640, https://doi.org/10.1021/ie0207919.
[2] B. Hjulström, S. Isaksson, A. Hennius, Organic geochemical evidence for pine tar production in middle Eastern Sweden during the Roman Iron Age, J. Archaeol. Sci. 33 (2) (2006) 283–294, https://doi.org/10.1016/j.jas.2005.06.017.
[3] A.V. Bridgwater, Review of fast pyrolysis of biomass and product upgrading, Biomass-.-. Bioenerg. 38 (2012) 68–94, https://doi.org/10.1016/j.biombioe.2011.01.048.
[4] X. Hu, M. Gholizadeh, Biomass pyrolysis: a review of the process development and challenges from initial researches up to the commercialisation stage, J. Energy Chem. 39 (2019) 109–143, https://doi.org/10.1016/j.jechem.2019.01.024.
[5] M.I. Jahirul, M.G. Rasul, A.A. Chowdhury, N. Ashwath, Biofuels production through biomass pyrolysis-a technological review, Energies 5 (12) (2012) 4952–5001, https://doi.org/10.3390/en5124952.
[6] T. Kan, V. Strezov, T.J. Evans, Lignocellulosic biomass pyrolysis: a review of product properties and effects of pyrolysis parameters, Renew. Sust. Energ. Rev. 57 (2016) 1126–1140, https://doi.org/10.1016/j.rser.2015.12.185.
[7] M.S. Mettler, D.G. Vlachos, P.J. Dauenhauer, Top ten fundamental challenges of biomass pyrolysis for biofuels, Energ. Environ. Sci. 5 (7) (2012) 7797–7809, https://doi.org/10.1039/C2EE21679E.
[8] D. Mohan, C.U. Pittman, P.H. Steele, Pyrolysis of wood/biomass for bio-oil: a critical review, Energ. Fuel 20 (3) (2006) 848–889, https://doi.org/10.1021/ef0502397.
[9] A. Oasmaa, J. Lehto, Y. Solantausta, S. Kallio, Historical review on VTT fast pyrolysis bio-oil production and upgrading, Energ. Fuel 35 (7) (2021) 5683–5695, https://doi.org/10.1021/acs.energyfuels.1c00177.
[10] G. Várhegyi, From "Sirups" to Biocarbons: a 30 year research cooperation for better biomass utilization with michael J. Antal, Jr, Energ. Fuel 30 (10) (2016) 7887–7895, https://doi.org/10.1021/acs.energyfuels.6b00860.
[11] G.Y. Wang, Y.J. Dai, H.P. Yang, Q.G. Xiong, K.G. Wang, J.S. Zhou, Y.C. Li, S. R. Wang, A review of recent advances in biomass pyrolysis, Energ. Fuel 34 (12) (2020) 15557–15578, https://doi.org/10.1021/acs.energyfuels.0c03107.
[12] S.R. Wang, G.X. Dai, H.P. Yang, Z.Y. Luo, Lignocellulosic biomass pyrolysis mechanism: a state-of-the-art review, Prog. Energ. Combust. 62 (2017) 33–86, https://doi.org/10.1016/j.pecs.2017.05.004.
[13] S. Williams, C. Higashi, P. Phothisantikul, S. Van Wesenbeeck, M.J. Antal, The fundamentals of biocarbon formation at elevated pressure: from 1851 to the 21st century, J. Anal. Appl. Pyrol. 113 (2015) 225–230, https://doi.org/10.1016/j.jaap.2014.12.021.
[14] J. Lédé, Cellulose pyrolysis kinetics: An historical review on the existence and role of intermediate active cellulose, J. Anal. Appl. Pyrol. 94 (2012) 17–32, https://doi.org/10.1016/j.jaap.2011.12.019.
[15] C. Serbanescu, Kinetic analysis of cellulose pyrolysis: a short review, Chem. Pap. 68 (7) (2014) 847–860, https://doi.org/10.2478/s11696-013-0529-z.
[16] D.F. Arseneau, Competitive reactions in thermal decomposition of cellulose (-&), Can. J. Chem. 49 (4) (1971) 632, https://doi.org/10.1139/v71-101.
[17] A.G.W. Bradbury, Y. Sakai, F. Shafizadeh, Kinetic-model for pyrolysis of cellulose, J. Appl. Polym. Sci. 23 (11) (1979) 3271–3280, https://doi.org/10.1002/app.1979.070231112.
[18] A. Broido, A.C. Javier-Son, A.C. Ouano, E.M. Barrall II, Molecular-weight decrease in early pyrolysis of crystalline and amorphous cellulose, J. Appl. Polym. Sci. 17 (12) (1973) 3627–3635, https://doi.org/10.1002/app.1973.070171207.
[19] A. Broido, M.A. Nelson, Char yield on pyrolysis of cellulose, Combust. Flame 24 (2) (1975) 263–268, https://doi.org/10.1016/0010-2180(75)90156-X.
[20] P.H. Brunner, P.V. Roberts, The significance of heating rate on char yield and char properties in the pyrolysis of cellulose, Carbon 18 (3) (1980) 217–224, https://doi.org/10.1016/0008-6223(80)90064-0.
[21] A.E. Lipska, W.J. Parker, Kinetics of the pyrolysis of cellulose in the temperature range 250-300 Degrees °C (-&), J. Appl. Polym. Sci. 10 (10) (1966) 1439, https://doi.org/10.1002/app.1966.070101005.
[22] A.E. Lipska, F.A. Wodley, Isothermal pyrolysis of cellulose - kinetics and gas chromatographic mass spectrometric analysis of degradation products (-&), J. Appl. Polym. Sci. 13 (5) (1969) 851, https://doi.org/10.1002/app.1969.070130504.
[23] V. Mamleev, S. Bourbigot, M. Le Bras, J. Yvon, The facts and hypotheses relating to the phenomenological model of cellulose pyrolysis Interdependence of the steps, J. Anal. Appl. Pyrol. 84 (1) (2009) 1–17, https://doi.org/10.1016/j.jaap.2008.10.014.
[24] G. Varhegyi, E. Jakab, M.J. Antal, Is the broido-shafizadeh model for cellulose pyrolysis true, Energ. Fuel 8 (6) (1994) 1345–1352, https://doi.org/10.1021/ef00048a025.
[25] N.D. Le, M. Trogen, Y.B. Ma, R.J. Varley, M. Hummel, N. Byrne, Cellulose-lignin composite fibers as precursors for carbon fibers: Part 2-The impact of precursor properties on carbon fibers, Carbohyd. Polym. 250 (2020) 116918, https://doi.org/10.1016/j.carbpol.2020.116918.
[26] J. Mikkilä, M. Trogen, K.A.Y. Koivu, J. Kontro, J. Kuuskeri, R. Maltari, Z. Dekere, M. Kemell, M.R. Mäkelä, P.A. Nousiainen, M. Hummel, J. Sipilä, K. Hildén, Fungal treatment modifies kraft lignin for lignin- and cellulose-based carbon fiber precursors, ACS Omega 5 (11) (2020) 6130–6140, https://doi.org/10.1021/acsomega.0c00142.
[27] M. Trogen, N.D. Le, D. Sawada, C. Guizani, T.V. Lourençon, L. Pitkänen, H. Sixta, R. Shah, H. O'Neill, M. Balakshin, N. Byrne, M. Hummel, Cellulose-lignin composite fibres as precursors for carbon fibres. Part 1-Manufacturing and properties of precursor fibres, Carbohyd. Polym. 252 (2021) 117133, https://doi.org/10.1016/j.carbpol.2020.117133.
[28] H. Zahra, D. Sawada, C. Guizani, Y.B. Ma, S. Kumagai, T. Yoshioka, H. Sixta, M. Hummel, Close packing of cellulose and chitosan in regenerated cellulose fibers improves carbon yield and structural properties of respective carbon fibers, Biomacromolecules 21 (10) (2020) 4326–4335, https://doi.org/10.1021/acs.biomac.0c01117.
[29] G. Dobele, G. Rossinskaja, G. Telysheva, D. Meier, O. Faix, Cellulose dehydration and depolymerization reactions during pyrolysis in the presence of phosphoric acid, J. Anal. Appl. Pyrol. 49 (1-2) (1999) 307–317, https://doi.org/10.1016/S0165-2370(98)00126-0.
[30] M. Jang, D. Choi, Y. Kim, H.S. Kil, S.K. Kim, S.M. Jo, S.H. Lee, S.S. Kim, Role of sulfuric acid in thermostabilization and carbonization of lyocell fibers, Cellulose 30 (12) (2023) 7633–7652, https://doi.org/10.1007/s10570-023-05404-4.
[31] D.Y. Kim, Y. Nishiyama, M. Wada, S. Kuga, High-yield carbonization of, Cellul. Sulfur. Acid. Impregn., Cellul. 8 (1) (2001) 29–33, https://doi.org/10.1023/A:1016621103245.
[32] Y. Long, Y. Yu, Y.W. Chua, H.W. Wu, Acid-catalysed cellulose pyrolysis at low temperatures, Fuel 193 (2017) 460–466, https://doi.org/10.1016/j.fuel.2016.12.067.
[33] M. Al Aiti, D. Jehnichen, D. Fischer, H. Brünig, G. Heinrich, On the morphology and structure formation of carbon fibers from polymer precursor systems, Prog. Mater. Sci. 98 (2018) 477–551, https://doi.org/10.1016/j.pmatsci.2018.07.004.
[34] A.G. Dumanli, A.H. Windle, Carbon fibres from cellulosic precursors: a review, J. Mater. Sci. 47 (10) (2012) 4236–4250, https://doi.org/10.1007/s10853-011-6081-8.
[35] T. Peijs, R. Kirschbaum, P.J. Lemstra, Chapter 5: a critical review of carbon fiber and related products from an industrial perspective, Adv. Ind. Eng. Poly. Res. 5 (2) (2022) 90–106, https://doi.org/10.1016/j.aiepr.2022.03.008.
[36] V. Piazza, R.B. da Silva Junior, A. Frassoldati, L. Lietti, S. Chiaberge, C. Gambaro, A. Siviero, T. Faravelli, A. Beretta, Detailed speciation of biomass pyrolysis products with a novel TGA-based methodology: the case-study of cellulose, J. Anal. Appl. Pyrol. 178 (2024) 106413, https://doi.org/10.1016/j.jaap.2024.106413.
[37] P. Jusner, M. Bacher, J. Simon, F. Bausch, H. Khaliliyan, S. Schiehser, I. Sumerskii, E. Schwaiger, A. Potthast, T. Rosenau, Analyzing the effects of thermal stress on insulator papers by solid-state ^{13}C NMR spectroscopy, Cellulose 29 (2) (2022) 1081–1095, https://doi.org/10.1007/s10570-021-04338-z.
[38] H. Knicker, M. Velasco-Molina, M. Knicker, 2D Solid-State HETCOR ^{1}H–^{13}C NMR experiments with variable cross polarization times as a tool for a better understanding of the chemistry of cellulose-based pyrochars-a tutorial, Appl. Sci. -Basel 11 (18) (2021), https://doi.org/10.3390/app11188569.
[39] I. Pastorova, R.E. Botto, P.W. Arisz, J.J. Boon, Cellulose char structure - a combined analytical Py-GC-MS, FTIR, and NMR-Study, Carbohyd. Res. 262 (1) (1994) 27–47, https://doi.org/10.1016/0008-6215(94)84003-2.
[40] H. Plaisantin, R. Pailler, A. Guette, G. Daudé, M. Pétraud, B. Barbe, M. Birot, J. P. Pillot, P. Olry, Conversion of cellulosic fibres into carbon fibres: a study of the mechanical properties and correlation with chemical structure, Compos. Sci. Technol. 61 (14) (2001) 2063–2068, https://doi.org/10.1016/S0266-3538(01)00107-5.
[41] M.M. Tang, R. Bacon, Carbonization of cellulose fibers 1. Low temperature pyrolysis (-&), Carbon 2 (3) (1964) 211, https://doi.org/10.1016/0008-6223(64)90035-1.
[42] J. Zawadzki, M. Wisniewski, ^{13}C NMR study of cellulose thermal treatment, J. Anal. Appl. Pyrol. 62 (1) (2002) 111–121, https://doi.org/10.1016/S0165-2370(00)00217-5.
[43] Y. Sekiguchi, J.S. Frye, F. Shafizadeh, Structure and formation of cellulosic chars, J. Appl. Polym. Sci. 28 (11) (1983) 3513–3525, https://doi.org/10.1002/app.1983.070281116.
[44] S.R. Wang, X.J. Guo, T. Liang, Y. Zhou, Z.Y. Luo, Mechanism research on cellulose pyrolysis by Py-GC/MS and subsequent density functional theory studies, Bioresour. Technol. 104 (2012) 722–728, https://doi.org/10.1016/j.biortech.2011.10.078.
[45] J.J. Liang, J. Chen, S.B. Wu, C. Liu, M. Lei, Comprehensive insights into cellulose structure evolution multi-perspective analysis during a slow pyrolysis process,

Sustain. Energ. Fuels 2 (8) (2018) 1855–1862, https://doi.org/10.1039/C8SE00166A.
[46] J.B. Wooten, J.I. Seeman, M.R. Hajaligol, Observation and characterization of cellulose pyrolysis intermediates by ^{13}C CPMAS NMR: a new mechanistic model, Energ. Fuel 18 (1) (2004) 1–15, https://doi.org/10.1021/ef0300601.
[47] G.J. Kwon, D.Y. Kim, K.Y. Kang, Effects of low-temperature pretreatment on carbonization of cellulose for the production of biocarbons, J. Korean Phys. Soc. 60 (10) (2012) 1814–1817, https://doi.org/10.3938/jkps.60.1814.
[48] A. Broido, M. Weinstein, Low Temperature Isothermal Pyrolysis of Cellulose, in: H. G. Wiedemann (Ed.), Thermal Analysis, Birkhäuser, Basel, 1972, pp. 285–296.
[49] J. Scheirs, G. Camino, W. Tumiatti, Overview of water evolution during the thermal degradation of cellulose, Eur. Polym. J. 37 (5) (2001) 933–942, https://doi.org/10.1016/S0014-3057(00)00211-1.
[50] M.J. Antal, Biomass Pyrolysis: A Review of the Literature Part 1–Carbohydrate Pyrolysis, in: D.K.W. Böer, J.A. (Eds.), Advances in Solar Energy, Springer, Boston, MA, 1983, pp. 61–111.
[51] H. Kawamoto, Review of reactions and molecular mechanisms in cellulose pyrolysis, Curr. Org. Chem. 20 (23) (2016) 2444–2457, https://doi.org/10.2174/1385272820666160525102910.
[52] L. Fliri, C. Guizani, I.Y. Miranda-Valdez, L. Pitkänen, M. Hummel, Reinvestigating the concurring reactions in early-stage cellulose pyrolysis by solution state NMR spectroscopy, J. Anal. Appl. Pyrol. 175 (2023) 106153, https://doi.org/10.1016/j.jaap.2023.106153.
[53] E.W. Leng, M. Costa, Y. Peng, Y. Zhang, X. Gong, A.Q. Zheng, Y.Q. Huang, M.H. Xu, Role of different chain end types in pyrolysis of glucose-based anhydro-sugars and oligosaccharides, Fuel 234 (2018) 738–745, https://doi.org/10.1016/j.fuel.2018.07.075.
[54] Q. Lu, B. Hu, Z.X. Zhang, Y.T. Wu, M.S. Cui, D.J. Liu, C.Q. Dong, Y.P. Yang, Mechanism of cellulose fast pyrolysis: The role of characteristic chain ends and dehydrated units, Combust. Flame 198 (2018) 267–277, https://doi.org/10.1016/j.combustflame.2018.09.025.
[55] S. Matsuoka, H. Kawamoto, S. Saka, Thermal glycosylation and degradation reactions occurring at the reducing ends of cellulose during low-temperature pyrolysis, Carbohyd. Res. 346 (2) (2011) 272–279, https://doi.org/10.1016/j.carres.2010.10.018.
[56] S. Matsuoka, H. Kawamoto, S. Saka, What is active cellulose in pyrolysis? An approach based on reactivity of cellulose reducing end, J. Anal. Appl. Pyrol. 106 (2014) 138–146, https://doi.org/10.1016/j.jaap.2014.01.011.
[57] H. Kawamoto, M. Murayama, S. Saka, Pyrolysis behavior of levoglucosan as an intermediate in cellulose pyrolysis: polymerization into polysaccharide as a key reaction to carbonized product formation, J. Wood Sci. 49 (5) (2003) 469–473, https://doi.org/10.1007/s10086-002-0487-5.
[58] M. Jang, L. Fliri, M. Trogen, D. Choi, J.H. Han, J. Kim, S.K. Kim, S. Lee, S.S. Kim, M. Hummel, Accelerated thermostabilization through electron-beam irradiation for the preparation of cellulose-derived carbon fibers, Carbon 218 (2024) 118759, https://doi.org/10.1016/j.carbon.2023.118759.
[59] I. Pastorova, P.W. Arisz, J.J. Boon, Preservation of D-glucose-oligosaccharides in cellulose chars, Carbohyd. Res. 248 (1993) 151–165, https://doi.org/10.1016/0008-6215(93)84123-N.
[60] J.B. Paine, Y.B. Pithawalla, J.D. Naworal, Carbohydrate pyrolysis mechanisms from isotopic labeling Part 4. The pyrolysis Of D-glucose: the formation of furans, J. Anal. Appl. Pyrol. 83 (1) (2008) 37–63, https://doi.org/10.1016/j.jaap.2008.05.008.
[61] A. Kruse, A. Funke, M.M. Titirici, Hydrothermal conversion of biomass to fuels and energetic materials, Curr. Opin. Chem. Biol. 17 (3) (2013) 515–521, https://doi.org/10.1016/j.cbpa.2013.05.004.
[62] S.W. Liu, Y.T. Zhu, Y.H. Liao, H.Y. Wang, Q.Y. Liu, L.L. Ma, C.G. Wang, Advances in understanding the humins: formation, prevention and application, Appl. Energy Combust. Sci. 10 (2022) 100062, https://doi.org/10.1016/j.jaecs.2022.100062.
[63] J.C.V. Calderón, J.S. Arora, S.H. Mushrif, Mechanistic investigation into the formation of humins in acid-catalyzed biomass reactions, ACS Omega 7 (49) (2022) 44786–44795, https://doi.org/10.1021/acsomega.2c04783.
[64] J. Heltzel, S.K.R. Patil, C.R.F. Lund, Humin Formation Pathways, in: M. Schlaf, Z. Zhang (Eds.), Reaction Pathways and Mechanisms in Thermocatalytic Biomass Conversion II, Springer, Singapore, 2016, pp. 105–118.
[65] S.K.R. Patil, J. Heltzel, C.R.F. Lund, Comparison of structural features of humins formed catalytically from glucose, fructose, and 5-hydroxymethylfurfuraldehyde, Energ. Fuel 26 (8) (2012) 5281–5293, https://doi.org/10.1021/ef3007454.
[66] S.K.R. Patil, C.R.F. Lund, Formation and growth of humins via aldol addition and condensation during acid-catalyzed conversion of 5-hydroxymethylfurfural, Energ. Fuel 25 (10) (2011) 4745–4755, https://doi.org/10.1021/ef2010157.
[67] C. Falco, N. Baccile, M.M. Titirici, Morphological and structural differences between glucose, cellulose and lignocellulosic biomass derived hydrothermal carbons, Green. Chem. 13 (11) (2011) 3273–3281, https://doi.org/10.1039/C1GC15742F.
[68] N. Paksung, J. Pfersich, P.J. Arauzo, D. Jung, A. Kruse, Structural effects of cellulose on hydrolysis and carbonization behavior during hydrothermal treatment, ACS Omega 5 (21) (2020) 12210–12223, https://doi.org/10.1021/acsomega.0c00737.
[69] M. Sevilla, A.B. Fuertes, The production of carbon materials by hydrothermal carbonization of cellulose, Carbon 47 (9) (2009) 2281–2289, https://doi.org/10.1016/j.carbon.2009.04.026.
[70] T.M.C. Hoang, E.R.H. van Eck, W.P. Bula, J.G.E. Gardeniers, L. Lefferts, K. Seshan, Humin based by-products from biomass processing as a potential carbonaceous source for synthesis gas production, Green. Chem. 17 (2) (2015) 959–972, https://doi.org/10.1039/C4GC01324G.
[71] R.L. Johnson, J.M. Anderson, B.H. Shanks, X.W. Fang, M. Hong, K. Schmidt-Rohr, Spectrally edited 2D ^{13}C–^{13}C NMR spectra without diagonal ridge for characterizing ^{13}C-enriched low-temperature carbon materials, J. Magn. Reason. 234 (2013) 112–124, https://doi.org/10.1016/j.jmr.2013.06.006.
[72] I. van Zandvoort, E.J. Koers, M. Weingarth, P.C.A. Bruijnincx, M. Baldus, B. M. Weckhuysen, Structural characterization of ^{13}C-enriched humins and alkali-treated ^{13}C humins by 2D solid-state NMR, Green. Chem. 17 (8) (2015) 4383–4392, https://doi.org/10.1039/C5GC00327J.
[73] I. van Zandvoort, Y.H. Wang, C.B. Rasrendra, E.R.H. van Eck, P.C.A. Bruijnincx, H. J. Heeres, B.M. Weckhuysen, Formation, molecular structure, and morphology of humins in biomass conversion: influence of feedstock and processing conditions, Chemsuschem 6 (9) (2013) 1745–1758, https://doi.org/10.1002/cssc.201300332.
[74] T. Nomura, E. Minami, H. Kawamoto, Hydroxymethylfurfural as an intermediate of cellulose carbonization, Chemistryopen 10 (6) (2021) 610–617, https://doi.org/10.1002/open.202000314.
[75] M.R. Nimlos, S.J. Blanksby, X.H. Qian, M.E. Himmel, D.K. Johnson, Mechanisms of glycerol dehydration, J. Phys. Chem. A 110 (18) (2006) 6145–6156, https://doi.org/10.1021/jp060597q.
[76] Y.C. Lin, J. Cho, G.A. Tompsett, P.R. Westmoreland, G.W. Huber, Kinetics and mechanism of cellulose pyrolysis, J. Phys. Chem. C. 113 (46) (2009) 20097–20107, https://doi.org/10.1021/jp906702p.
[77] S.C. Yuan, M.V. Tyufekchiev, M.T. Timko, K. Schmidt-Rohr, Direct quantification of the degree of polymerization of hydrolyzed cellulose by solid-state NMR spectroscopy, Cellulose 29 (4) (2022) 2131–2144, https://doi.org/10.1007/s10570-022-04433-9.
[78] J.M. Spörl, R. Beyer, F. Abels, T. Cwik, A. Müller, F. Hermanutz, M.R. Buchmeiser, Cellulose-derived carbon fibers with improved carbon yield and mechanical properties, Macromol. Mater. Eng. 302 (10) (2017), https://doi.org/10.1002/mame.201700195.
[79] K. Heise, T. Koso, L. Pitkänen, A. Potthast, A.W.T. King, M.A. Kostiainen, E. Kontturi, Knoevenagel condensation for modifying the reducing end groups of cellulose nanocrystals, ACS Macro. Lett. 8 (12) (2019) 1642–1647, https://doi.org/10.1021/acsmacrolett.9b00838.
[80] C. Guizani, O. Sorsa, V. Siipola, T. Ohra-Aho, R. Paalijärvi, A. Pasanen, M. Mäkelä, A. Kalliola, M. Vilkman, K. Torvinen, The effects of lignin structure on the multiscale properties and electrochemical performance of activated carbons, Biomass-.-. Conv. Bioref. (2023), https://doi.org/10.1007/s13399-023-04373-9.
[81] M. Maciejewski, A. Baiker, Quantitative calibration of mass spectrometric signals measured in coupled TA-MS system, Thermochim. Acta 295 (1-2) (1997) 95–105, https://doi.org/10.1016/S0040-6031(97)00100-7.
[82] L. Fliri, K. Heise, T. Koso, A.R. Todorov, D.R. del Cerro, S. Hietala, J. Fiskari, I. Kilpeläinen, M. Hummel, A.W.T. King, Solution-state nuclear magnetic resonance spectroscopy of crystalline cellulosic materials using a direct dissolution ionic liquid electrolyte, Nat. Protoc. 18 (7) (2023) 2084–2123, https://doi.org/10.1038/s41596-023-00832-9.
[83] J. Klepp, W. Dillon, Y. Lin, P. Feng, B.W. Greatrex, Preparation of (-)-levoglucosenone from cellulose using sulfuric acid in polyethylene glycol, Org. Synth. 97 (2020) 38, https://doi.org/10.15227/orgsyn.097.0038.
[84] F. Shafizadeh, R.H. Furneaux, T.T. Stevenson, Some reactions of levoglucosenone, Carbohyd. Res. 71 (1) (1979) 169–191, https://doi.org/10.1016/S0008-6215(00)86069-3.
[85] M.A. Kougioumtzis, A. Marianou, K. Atsonios, C. Michailof, N. Nikolopoulos, N. Koukouzas, K. Triantafyllidis, A. Lappas, E. Kakaras, Production of 5-HMF from Cellulosic Biomass: experimental results and integrated process simulation, Waste Biomass-.-. Valor 9 (12) (2018) 2433–2445, https://doi.org/10.1007/s12649-018-0267-0.
[86] A. Mukherjee, M.J. Dumont, V. Raghauan, Review: Sustainable production of hydroxymethylfurfural and levulinic acid: challenges and opportunities, Biomass-.-. Bioenerg. 72 (2015) 143–183, https://doi.org/10.1016/j.biombioe.2014.11.007.
[87] C. Falco, F.P. Caballero, F. Babonneau, C. Gervais, G. Laurent, M. Titirici, N. Baccile, Hydrothermal carbon from biomass: structural differences between hydrothermal and pyrolyzed carbons via ^{13}C solid state NMR, Langmuir 27 (23) (2011) 14460–14471, https://doi.org/10.1021/la202361p.
[88] W.J. Liu, H. Jiang, H.Q. Yu, Development of biochar-based functional materials: toward a sustainable platform carbon material, Chem. Rev. 115 (22) (2015) 12251–12285, https://doi.org/10.1021/acs.chemrev.5b00195.
[89] Y. Le Brech, L. Delmotte, J. Raya, N. Brosse, R. Gadiou, A. Dufour, High Resolution solid state ^{2}D NMR analysis of biomass and biochar, Anal. Chem. 87 (2) (2015) 843–847, https://doi.org/10.1021/ac504237c.
[90] R.C. Cioc, M. Crockatt, J.C. Waal, P.C.A. Bruijnincx, The Interplay between Kinetics and Thermodynamics in Furan Diels-Alder Chemistry for Sustainable Chemicals Production, Angew. Chem. Int. Ed. 61 (17) (2022) e202114720, https://doi.org/10.1002/anie.202114720.
[91] Y.T. Cheng, G.W. Huber, Chemistry of furan conversion into aromatics and Olefins over HZSM-5: a model biomass conversion reaction, ACS Catal. 1 (6) (2011) 611–628, https://doi.org/10.1021/cs200103j.
[92] C.C. Chang, S.K. Green, C.L. Williams, P.J. Dauenhauer, W. Fan, Ultra-selective cycloaddition of dimethylfuran for renewable -xylene with H-BEA, Green. Chem. 16 (2) (2014) 585–588, https://doi.org/10.1039/C3GC40740C.
[93] I.F. Teixeira, B.T.W. Lo, P. Kostetskyy, L. Ye, C.C. Tang, G. Mpourmpakis, S.C. E. Tsang, Direct catalytic conversion of biomass-derived furan and ethanol to ethylbenzene, ACS Catal. 8 (3) (2018) 1843–1850, https://doi.org/10.1021/acscatal.7b03952.